

FLASH MIXING ON THE WHITE DWARF COOLING CURVE: UNDERSTANDING HOT HORIZONTAL BRANCH ANOMALIES IN NGC 2808¹

THOMAS M. BROWN^{2,3}, ALLEN V. SWEIGART, THIERRY LANZ⁴, WAYNE B. LANDSMAN⁵, IVAN HUBENY²,

Laboratory for Astronomy & Solar Physics, Code 681, NASA/GSFC, Greenbelt, MD 20771.
tbrown@stsci.edu, sweigart@bach.gsfc.nasa.gov, lanz@nova.gsfc.nasa.gov, landsman@mpb.gsfc.nasa.gov,
hubeny@tustly.gsfc.nasa.gov

To appear in The Astrophysical Journal

ABSTRACT

We present an ultraviolet color-magnitude diagram (CMD) spanning the hot horizontal branch (HB), blue straggler, and white dwarf populations of the globular cluster NGC 2808. These data were obtained with the far-UV and near-UV cameras on the Space Telescope Imaging Spectrograph (STIS). Although previous optical CMDs of NGC 2808 show a high temperature gap within the hot HB population, no such gap is evident in our UV CMD. Instead, we find a population of hot subluminal HB stars, an anomaly only previously reported for the globular cluster ω Cen. Our theoretical modeling indicates that the location of these subluminal stars in the UV CMD, as well as the high temperature gap along the HB in optical CMDs, can be explained if these stars underwent a late helium-core flash while descending the white dwarf cooling curve. We show that the convection zone produced by such a late helium flash will penetrate into the hydrogen envelope, thereby mixing hydrogen into the hot helium-burning interior, where it is rapidly consumed. This phenomenon is analogous to the “born again” scenario for producing hydrogen-deficient stars following a late helium-shell flash. The flash mixing of the envelope greatly enhances the envelope helium and carbon abundances, and leads, in turn, to a discontinuous increase in the HB effective temperatures at the transition between canonical and flash-mixed stars. We argue that the hot HB gap is associated with this theoretically predicted dichotomy in the HB properties. Moreover, the changes in the emergent spectral energy distribution caused by these abundance changes are primarily responsible for explaining the hot subluminal HB stars. Although further evidence is needed to confirm that a late helium-core flash can account for the subluminal HB stars and the hot HB gap, we demonstrate that an understanding of these stars requires the use of appropriate theoretical models for their evolution, atmospheres, and spectra.

Subject headings: globular clusters: individual (NGC 2808) – stars: evolution – stars: horizontal branch – ultraviolet: stars – ultraviolet: atmospheric effects

1. INTRODUCTION

The horizontal branch (HB) represents the core helium-burning phase of stellar evolution for low-mass stars. This late phase of stellar evolution is named for its theoretical locus in the HR diagram, which spans a much wider range in temperature than in bolometric luminosity. The observed temperature distribution of HB stars tends to become redder at increasing metallicity, and thus metallicity is generally regarded as the “first parameter” of HB morphology. However, the existence of clusters with similar metallicities but very distinct HB morphologies has led to the “second parameter” debate. Indeed, Rich et al. (1997) have recently shown that even metal-rich globular clusters can have extended blue HBs. It is well-known that multiple parameters can potentially act as second parameters on the HB (e.g., age, mass loss, helium abundance, rotation, cluster dynamics; Fusi Pecci & Bellazzini 1997). Although all of these parameters can theoretically govern HB morphology, it remains to be seen which of them actually plays a dominant role.

¹Based on observations with the NASA/ESA Hubble Space Telescope obtained at the Space Telescope Science Institute, which is operated by AURA, Inc., under NASA contract NAS 5-26555.

²NOAO

³Now at the Space Telescope Science Institute, 3700 San Martin Drive, Baltimore, MD 21218.

⁴University of Maryland

⁵Raytheon ITSS

Besides the second parameter effect, there are many other intriguing peculiarities in the HB morphology that still defy explanation. Some globular clusters possess bimodal HBs with substantial populations of both “blue” HB (BHB) stars hotter than the instability strip, and “red” HB (RHB) stars cooler than the instability strip, but with very few stars in between. In some clusters one finds a long blue HB trail, often punctuated by gaps, that extends to the “extreme” HB (EHB) stars, which are defined in this paper as HB stars with effective temperatures $T_{\text{eff}} \gtrsim 20,000$ K. These EHB stars correspond to the subdwarf B (sdB) stars studied in the Galactic field population (e.g., Saffer et al. 1994). Another peculiarity has been reported by D’Cruz et al. (2000), who found a population of subluminal HB stars in ω Cen.

The HB is not simply a sequence in T_{eff} – it is also a sequence in envelope mass (M_{env}). Stars with large M_{env} occupy the RHB, while stars with small M_{env} occupy the EHB. In theory, the range in M_{env} can result from a range in red-giant-branch (RGB) mass loss. However, it is difficult to see how one mechanism alone can produce the entire range of HB stars. A low-mass star would have to lose several tenths of a solar mass on the RGB, while retaining an envelope mass of just a few hundredths of a solar mass, in order to arrive on the hot end of the zero-age HB (ZAHB) via the same process that produces stars on the cool end of the ZAHB. Furthermore, the gaps on the HB would then imply “forbidden” values of mass loss and/or envelope mass. Historically, populating the entire HB via one mechanism has implied an unpalatable fine-tuning of the mass-

loss process. Instead, there may be distinct physical processes populating different temperature ranges on the HB (see, e.g., Ferraro et al. 1998). Peculiarities in HB morphology, such as gaps and subluminous stars, may be important clues to these formation mechanisms.

In this paper, we analyze new ultraviolet images of NGC 2808, a globular cluster that has been well-studied because of its unusual HB morphology. NGC 2808 was one of the first clusters known to have a bimodal HB, with a large gap between the BHB and RHB stars (Harris 1974) and only 2 known RR Lyrae (Clement & Hazen 1989). Rood et al. (1993) have pointed out that NGC 2808 may even be an example of the second parameter effect operating within a single cluster. Although NGC 2808 is of intermediate metallicity ($[Fe/H] = -1.36$; Walker 1999), it possesses one of the longest blue HB tails of any globular cluster. Moreover, there are two striking gaps within this blue tail: one between the EHB and BHB, and another within the EHB itself (Sosin et al. 1997; Walker 1999; Bedin et al. 2000); the colors of the gaps imply effective temperatures of 17,000 K and 25,000 K, respectively, if the color-temperature transformation employs synthetic spectra at the cluster metallicity. Although unusual, HB gaps are not unique to NGC 2808; gaps have also been found in many other globular clusters (e.g., M13, M80, and NGC 6273; Ferraro et al. 1998; Piotto et al. 1999), while Whitney et al. (1994, 1998) and D’Cruz et al. (2000) have reported both gaps and subluminous stars in the HB population of ω Cen. Our UV images of NGC 2808 confirm the presence of a pronounced gap between the EHB and BHB, but not the gap seen within the EHB in optical color magnitude diagrams (CMDs). Instead, we find a substantial population of subluminous EHB stars. In this paper, we will present a new theoretical scenario for understanding these peculiarities of the EHB population in NGC 2808, as well as ω Cen.

D’Cruz et al. (2000) and Whitney et al. (1998) claimed that the hot subluminous stars on the HB of ω Cen were probably a population of “blue-hook” HB stars. These are stars that experience a late helium-core flash. Normally, stars ignite He burning at the tip of the RGB, but if they undergo very high mass-loss, the stars will leave the RGB and ignite He burning while descending the white dwarf (WD) cooling curve (Castellani & Castellani 1993). D’Cruz et al. (1996) suggested that such stars provide another avenue for populating the hot end of the HB, thus helping to alleviate the fine-tuning problem. In their scenario, the He-burning stars that arise from such a late flash should form a “blue-hook” appended to the hot end of the canonical EHB, with slightly lower core masses (by $\sim 0.01 M_{\odot}$) than those stars that arrive on the ZAHB directly from the RGB. D’Cruz et al. (2000) claimed that blue-hook stars should lie up to 0.1 mag below the EHB, but the subluminous HB stars in their CMD of ω Cen lie up to ~ 0.7 mag below the canonical EHB and, in addition, span a wide range in color, demonstrating that this idea needs further exploration.

Sweigart (1997) has shown that when stars undergo a late helium-core flash on the WD cooling curve, flash mixing of the hydrogen envelope with the helium core will greatly enhance the envelope helium and carbon abundances. At the peak of the flash, the He-burning luminosity (L_{He}) reaches $10^{10} L_{\odot}$. Normally, the flash convection produced by such a high burning rate does not penetrate the hydrogen shell; however, when stars ignite He on the WD cooling curve, they do so in the presence of a much weaker hydrogen-burning shell. The lower entropy barrier associated with this weaker hydrogen-burning

shell (Iben 1976) allows the flash convection to penetrate the hydrogen envelope, thereby mixing hydrogen into the hot He-burning interior, where it is rapidly consumed. The result is a hydrogen-deficient He-burning star with enhanced helium and carbon in the envelope. A similar process has been proposed to explain the extremely hydrogen-deficient R Coronae Borealis (R CrB) stars (also known as “born again” stars), whereby the envelope hydrogen is mixed inward during a very late helium-shell flash (e.g., Renzini 1990). This flash mixing might also explain the enhanced helium abundances seen in some field sdO stars (Lemke et al. 1997) and a small fraction of the field sdB stars (e.g., Moehler et al. 1990). Because flash mixing produces envelope abundances that are very distinct from those in canonical EHB stars, the stellar atmospheres used for the models of blue-hook stars should include these abundance changes when predicting their observed colors and luminosities.

In this paper, we will examine new observations of NGC 2808, taken with the Space Telescope Imaging Spectrograph (STIS) on board the Hubble Space Telescope (HST). In §2, we describe the observations, data reduction, and photometry. We then present the UV CMD in §3, revealing a population of stars below the canonical ZAHB, a phenomenon previously seen only in ω Cen. In §4, we present the stellar evolutionary tracks we use to investigate the HB morphology, with special attention to models with flash mixing on the WD cooling curve. The atmospheres of flash-mixed stars are expected to have hydrogen-poor, non-solar scaled abundances; our adopted model atmospheres with these abundances are discussed in §5. In §6, we first rule out several alternative scenarios for understanding the hot sub-ZAHB stars, and then conclude that flash mixing provides the most likely explanation. We then demonstrate, in §7, that the dichotomy between the flash-mixed stars and the canonical ZAHB can account for the EHB gap seen in optical CMDs of NGC 2808. We consider some implications of the flash-mixing scenario in §8. We then review our conclusions in §9.

2. OBSERVATIONS AND DATA REDUCTION

2.1. Imaging

Because NGC 2808 provides a well-sampled field of hot stars, the cluster was observed with STIS in order to provide a geometric distortion correction for the STIS camera modes. Although the observation plan was driven by the calibration goals, such calibration data, which are made immediately available to the public, can also be of scientific interest. Images were obtained in the far-UV crystal quartz (FUV/F25QTZ; pivot wavelength 1600 Å), near-UV 2700 Å continuum (NUV/F25CN270), and clear CCD (CCD/50CCD; pivot wavelength 5850 Å) modes, employing a cross-shaped dither pattern. The UV images were taken in the cluster center, but most of the CCD images were offset from the cluster center, to image a less crowded field. The CCD images obtained in the center are too crowded for useful photometry; we do not include them in our analysis, and employ them only to provide a third color for a false-color image of the cluster center. For the UV images that are the focus of this paper, the resulting sky coverage is almost three times larger than a single STIS exposure, but the depth of this coverage is very nonuniform, due to the overlapping coverage between individual exposures. Nonetheless, hot stars on and near the horizontal branch are well-detected in single exposures, so this varying depth only significantly affects the detection and measurement of stars that

are on the RHB or much fainter than the ZAHB. The observational parameters for the UV images are summarized in Table 1. The exposure times reflect the total amount of time observing in each mode (not the exposure depth at any one point in the image). A subsection of the STIS images is shown in Figure 1. The UV bandpasses are shown in Figure 2.

TABLE 1: UV Imaging

STIS band	Exp. (sec)	Observation date (2000)	coverage (\square'')
FUV/F25QTZ	8916	Jan 18 & Feb 16	1744
NUV/F25CN270	8906	Jan 19 & Feb 20	1752

The UV detectors employed by STIS are multi-anode microchannel arrays (MAMAs) with very little red leak. The MAMAs are also photon counters that register less than one count per incident cosmic ray; thus, cosmic ray rejection is not required for the UV imaging. For the CCD imaging (where an incident cosmic ray causes a massive many-count “hit”), we employed standard cosmic-ray rejection. A full description of the instrument and its capabilities can be found in Woodgate et al. (1998) and Kimble et al. (1998).

As explained above, the individual exposures were obtained in a cross-shaped dither pattern spanning the center of the cluster. Thus, we needed to rotate and register them before co-adding. The plate scale for the far-UV and near-UV modes differs slightly, but both are within a few percent of $0.025'' \text{ pix}^{-1}$. The plate scale of the CCD images is $0.05'' \text{ pix}^{-1}$. Using the DRIZZLE package (Fruchter & Hook 1998) in IRAF, we drizzled the individual exposures in each mode to the same plate scale (exactly $0.025'' \text{ pix}^{-1}$), including a correction for the geometric distortion. We then cross-correlated those images to solve for relative rotation and offsets, and then re-drizzled the original 1024×1024 pixel exposures to create a summed 2048×2048 pixel image for each band. The drizzling included masks for occulted corners and edges of the detector, plus hot and defective pixels.

Spectroscopic monitoring of the STIS UV modes has shown a small ($\lesssim 2\%$) variation in the near-UV sensitivity over the course of almost three years, with no net loss of sensitivity. However, the far-UV spectroscopic sensitivity has shown a small net decline (Bohlin 1999); this decline is somewhat wavelength dependent, ranging from 0.8%–2.8% per year across the entire far-UV wavelength range. The near-UV sensitivity variations are small enough to be ignored, but to minimize systematic errors, we derived a new far-UV imaging throughput curve for the date of our far-UV exposures. This new throughput curve is the product of the nominal throughput curve and the spectroscopic sensitivity drop as of 1 Feb 2000. This date is midway between the two sets of far-UV exposures, taken a month apart (see Table 1); the change in the sensitivity over that month is insignificant. A flat F_λ spectrum produces 7% fewer counts with the new far-UV sensitivity curve, compared to the nominal curve. Our revised far-UV imaging bandpass is shown in Figure 2, and it will be used to translate the theoretical stellar models to the observational plane.

2.2. Spectroscopy

The brightest star in these images was also observed spectroscopically with STIS on 20 April 1999. This star is located $\sim 18''$ from the cluster center; in Figure 1, it is the bright blue star on the upper right. The observations were taken as part of a spectroscopic followup program (HST Guest Observer program

7436) of post-asymptotic giant branch (post-AGB) candidates discovered on globular cluster images obtained with the Ultraviolet Imaging Telescope (UIT; Landsman et al. 2001). The spectroscopy was obtained through the $52'' \times 0.2''$ slit in the G140L, G230L, and G430L modes, providing wavelength coverage from 1150 Å to 5700 Å.

We reduced the spectroscopic data with the CALSTIS package of the STIS Instrument Definition Team (Lindler 1999). The star is sufficiently bright and isolated to allow the use of the standard extraction slit for the source (11 pixels). The reduced spectrum is shown in Figure 2. We use this spectrum to tie our photometry to an absolute flux scale, as described in the next section.

2.3. Photometry

Because both colors and luminosities are needed for the CMD, we are only interested in photometry for stars that are well-detected in both the far-UV and near-UV bands. To create a coordinate list of stars in the STIS images, we centroided on each star detected by eye in the far-UV image. The far-UV image is sparsely populated, and it has nonuniform coverage with varying signal-to-noise ratio, so this yielded much better results than an automated detection algorithm.

Once we had an object list for the cluster, we used the IRAF routine PHOT in the DIGIPHOTX/DAOPHOTX package to perform small-aperture photometry. The object aperture radius was 4 pixels, and the sky annulus spanned radii of 4–10 pixels. The sky annulus thus included a small predictable amount of source flux from each target star, but more accurately reflected the local background from the wings of neighboring stars. Because STIS is optimized for spectroscopy instead of imaging, the point spread function (PSF) varies as a function of horizontal position in a given exposure; our final images are the sum of many dithered exposures, which tends to average out the variations in the PSF, but use of an object aperture radius smaller than 4 pixels would increase the photometric scatter. To put the NGC 2808 photometry on an absolute scale, we used our spectrum of the UV-bright post-AGB star in the cluster (see Figure 2) to predict the imaging count rate for this star, because the spectroscopic sensitivity is far easier to calibrate than imaging sensitivity (through comparison with WD spectra). Comparison to the measured imaging count rate gave an aperture correction of 1.83 for the FUV/F25QTZ photometry and 1.44 for the NUV/F25CN270 photometry. Note that these aperture corrections account for both the encircled energy within the source aperture and also the subtraction of source light included in the sky annulus. Based upon an analysis of the STIS point spread function (PSF; Robinson 1997), the near-UV aperture correction is 2% smaller than expected, while the far-UV aperture correction is 6% larger than expected. The larger far-UV discrepancy reflects telescope breathing and systematic uncertainties in the imaging calibration at the $\lesssim 0.1$ mag level. We felt that normalization to this stellar spectrum would provide a more accurate photometric scale. In any case, the differences between our aperture correction and the nominal corrections for the STIS PSF are small.

Magnitudes for our photometry are in the STMAG system:

$$m = -2.5 \times \log_{10} f_\lambda - 21.10$$

$$f_\lambda = \text{counts} \times \text{PHOTFLAM} / \text{EXPTIME}$$

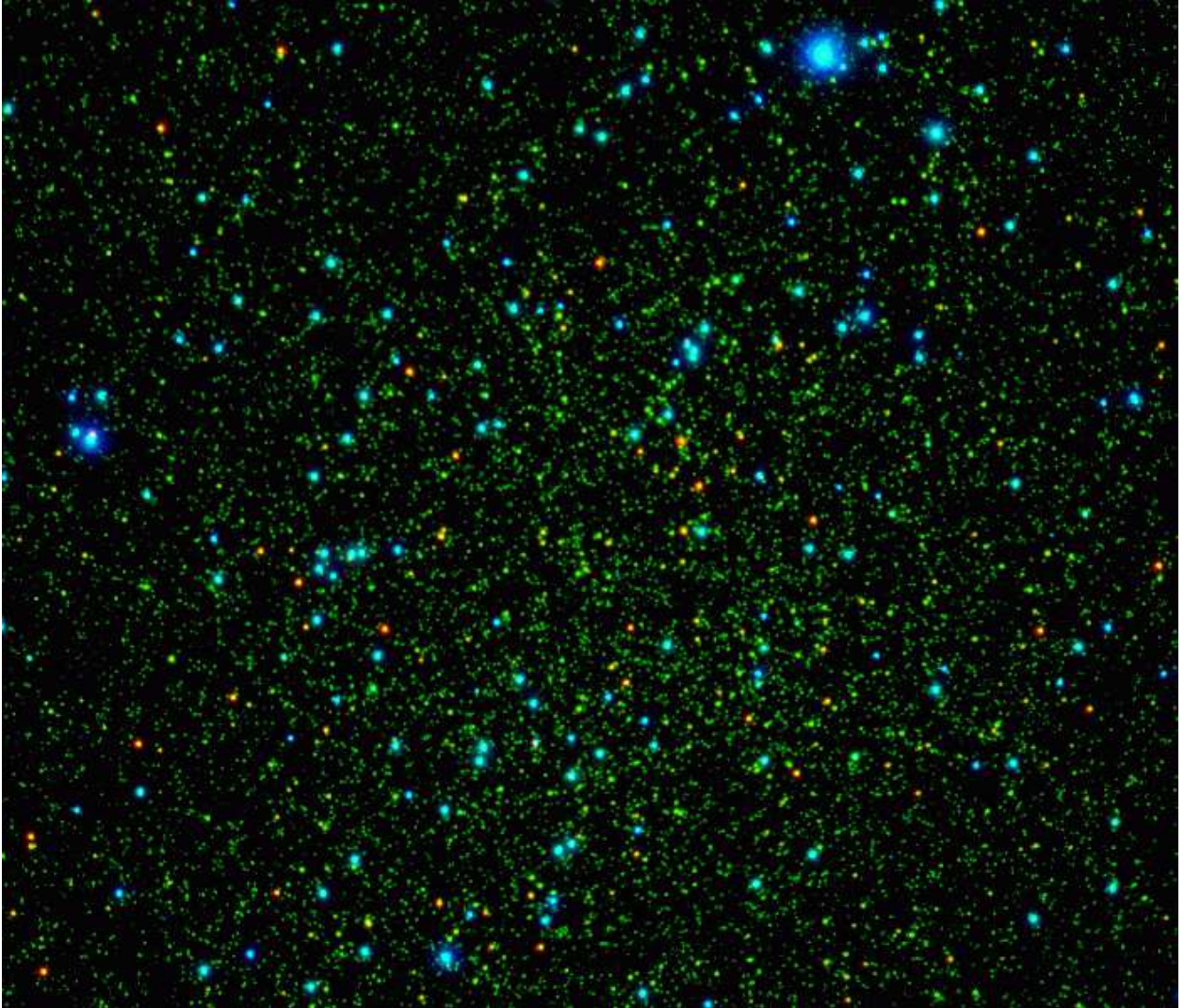


FIG. 1— STIS observations of the evolved stellar populations in the center of NGC 2808. This false-color image is the result of assigning the STIS far-UV image to the blue channel, the near-UV image to the green channel, and the optical CCD image to the red channel. The image has been cropped to $35'' \times 30''$ for display purposes. The population is well-resolved at the center of this dense cluster. We have also obtained UV-to-optical spectroscopy of the bright blue post-AGB star near the top of the image (see Figure 2).

where EXPTIME is the exposure time, and PHOTFLAM is $1.11 \times 10^{-16} \text{ erg s}^{-1} \text{ cm}^2 \text{ \AA}^{-1} / (\text{cts s}^{-1})$ for the FUV/F25QTZ filter, and $3.29 \times 10^{-17} \text{ erg s}^{-1} \text{ cm}^2 \text{ \AA}^{-1} / (\text{cts s}^{-1})$ for the NUV/F25CN270 filter. Note that this PHOTFLAM for the far-UV filter takes into account the 7% reduction in far-UV sensitivity.

Our photometric catalog contains 295 stars with $m_{FUV} \leq 22$ mag, $m_{NUV} \leq 22$ mag, and photometric errors ≤ 0.2 mag; the catalog is available in Table 2. The far-UV image is very sparsely populated, with fewer than one star per 1000 resolution elements to a depth of $m_{FUV} = 22$ mag. The near-UV image is fairly crowded, but not to an extent that affects our photometry. If automated object detection and photometry are done on the near-UV image (instead of using the position catalog derived from the far-UV), we find that there are fewer than one star per 30 resolution elements to a depth of $m_{NUV} = 22$ mag, fewer than one star per 55 resolution elements to a depth of $m_{NUV} = 21$ mag, and fewer than one star per 300 resolution elements to a depth of $m_{NUV} = 20$ mag.

3. ULTRAVIOLET COLOR MAGNITUDE DIAGRAM

We present the STIS photometry as a CMD in Figure 3. The data are shown as error bars, and the theoretical fiducials are shown as labeled grey curves. The exposure depth is variable across the image, so the photometric errors do not uniformly increase toward fainter magnitudes, but all stars on or near the HB are well-detected. The EHB and BHB stars fall into two distinct clumps, with 75 stars and 128 stars, respectively. White dwarf and blue straggler (BS) stars are also present. Below, we review the cluster parameters, evolutionary models, and synthetic spectra that drive the location of the theoretical fiducials. We then point out peculiarities in our CMD, and in the subsequent sections explore the theoretical interpretation in more detail.

3.1. Cluster Parameters

The metallicity, distance modulus, and foreground extinction are somewhat uncertain for NGC 2808, and have been examined extensively in the literature (e.g., Walker 1999 and refer-

ences therein). Walker (1999) makes a compelling case that $[\text{Fe}/\text{H}] = -1.36 \pm 0.05$ on the Zinn & West (1984) metallicity scale (see also Rutledge, Hesser, & Stetson 1997; Ferraro et al. 1999), and that is the value we will adopt here. Recently, Bedin et al. (2000) calculated the extinction and distance modulus for this cluster using several different methods and metallicity assumptions. When assuming the Zinn & West (1984) metallicity scale, they found that the distribution of RGB stars implies $E(B - V) = 0.18 \pm 0.01$ and $(m - M)_V = 15.60 \pm 0.10$. These are the values we will adopt here, which give good agreement between the theoretical and observed BHB locus. We apply this foreground reddening to all of the synthetic spectra using the Cardelli, Clayton, & Mathis (1989) parameterization. Assuming $A_V = 3.1 \times E(B - V) = 0.56$ mag, this gives $(m - M)_o = 15.04$ and a distance of 10.2 kpc.

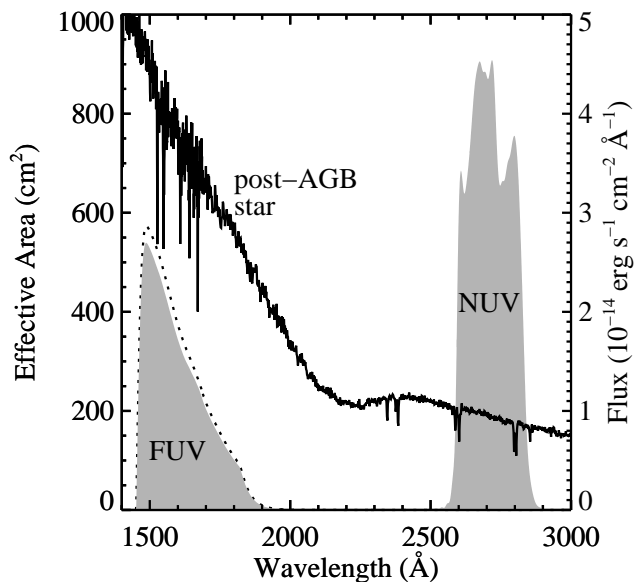


FIG. 2— STIS far-UV and near-UV bandpasses (grey filled areas; left-hand scale) used for the NGC 2808 imaging. The dotted line shows the nominal far-UV bandpass at the start of the STIS mission; at the time of the NGC 2808 imaging, the sensitivity was degraded by 7%. We also show a portion of the spectrum for the post-AGB star observed in NGC 2808 (right-hand scale), used to ensure that our aperture photometry was on an absolute flux scale.

3.2. White Dwarfs

White dwarfs are not the focus of this paper, but their possible presence in Figure 3 will be of interest to some readers. To distinguish stars that may lie on the WD cooling curve, we employed the 0.5 and 0.6 M_{\odot} C/O-core sequences of Wood (1995), representing DA WD stars (the actual WD stars in NGC 2808 are likely to have a mass near 0.55 M_{\odot}). To translate the WD sequence to the observational plane, we used the TLUSTY model atmosphere code (Hubeny & Lanz 1995) to calculate a sequence of non-LTE, pure hydrogen model atmospheres, and then used the SYNPEC spectra synthesis code (Hubeny, Lanz & Jeffery 1994) to calculate spectra. This was done for temperatures hotter than 20,000 K in the 0.5 and 0.6 M_{\odot} cooling curve sequences (at cooler temperatures, these sequences fall below the detection limits in our CMD). The synthetic spectra have no lines other than those of hydrogen.

If high RGB mass-loss does indeed drive the hot HB morphology in NGC 2808, the cluster might also contain a population of helium-core white dwarfs that never core flash. A

helium-core WD would have a larger radius than a C/O-core WD at the same T_{eff} (e.g., Panei, Althaus, & Benvenuto 2000). Unfortunately, because the WD cooling tracks in the STIS CMD (Figure 3) are nearly vertical, the helium WD cooling tracks of Panei et al. (2000) are indistinguishable from the C/O-core cooling tracks already plotted. Note that the presence of helium WDs in NGC 2808 might provide a counterexample to the usual assumption that helium WDs can only be formed as the products of binary evolution.

3.3. Blue Stragglers

The BS sequence in NGC 2808 has been seen clearly in previous optical CMDs, and the brightest blue stragglers are also present in the STIS data. The BS sequence should roughly follow the zero-age main sequence (ZAMS) up to twice the turnoff mass, if BS stars are the result of mergers between two MS stars. The MS turnoff mass in NGC 2808 is approximately 0.85 M_{\odot} , and well below the detection limits in our UV images, but stars near twice the turnoff mass are easily detectable in our STIS images. To highlight the BS sequence in these clusters, we used an isochrone from Bertelli et al. (1994), at $[\text{Fe}/\text{H}] = -1.3$ and an age of 4 Myr, truncating the isochrone at 1.7 M_{\odot} . The faintest part of the ZAMS shown in the CMD corresponds to 1.2 M_{\odot} . Assuming the nominal cluster abundances, we used the Kurucz (1993) grid of LTE synthetic spectra to translate the ZAMS to the observational plane, interpolating in effective temperature and metallicity from the grid points that most closely matched each point along the ZAMS. Note that depending upon the formation mechanism, blue straggler stars might have unusual surface abundances (e.g., Baily 1992), which would produce scatter away from the theoretical ZAMS.

3.4. Horizontal Branch Stars

Of primary concern in this paper is the distribution of HB stars in our UV CMD. The theoretical HB fiducials in Figure 3 come from our own calculations, which are discussed extensively in §4 and §5. These fiducials assume canonical evolution from the main sequence to the core He-burning phase, and were translated to the observational plane with synthetic spectra at the cluster metallicity. The lower bound of the canonical HB locus is the zero-age HB. The upper bound of the canonical HB locus marks the point where the star has completed 99% of its core He-burning lifetime; beyond this point, the evolution proceeds relatively rapidly, so that few stars would be expected.

In the UV, the HB morphology of NGC 2808 shares several features with CMDs at longer wavelengths, but also shows significant differences. The gap between the EHB and BHB, at $m_{\text{FUV}} - m_{\text{NUV}} \sim -1$ mag, is well detected, as is the gap between the BHB and RHB, at $m_{\text{FUV}} - m_{\text{NUV}} > 0$ mag. In fact, because the temperature scale is greatly stretched as one goes to cooler T_{eff} , the BHB-RHB gap is exaggerated, and the RHB stars are not detected at these wavelengths. However, the gap within the EHB (Sosin et al. 1997; Walker 1999; Bedin et al. 2000) is not present in our UV CMD. Instead, the EHB in the UV has a much larger luminosity width than the theoretical EHB, with many stars falling well below the theoretical EHB. Out of a total EHB population of 75 stars in Figure 3, 29 lie within the canonical EHB locus, while 46 are subluminal.

Given the large number of EHB stars, one expects to find a population of post-HB progeny. There are, in fact, 6 hot stars in our CMD that lie at luminosities far above the HB. The brightest is a post-AGB star, for which we have obtained UV-optical

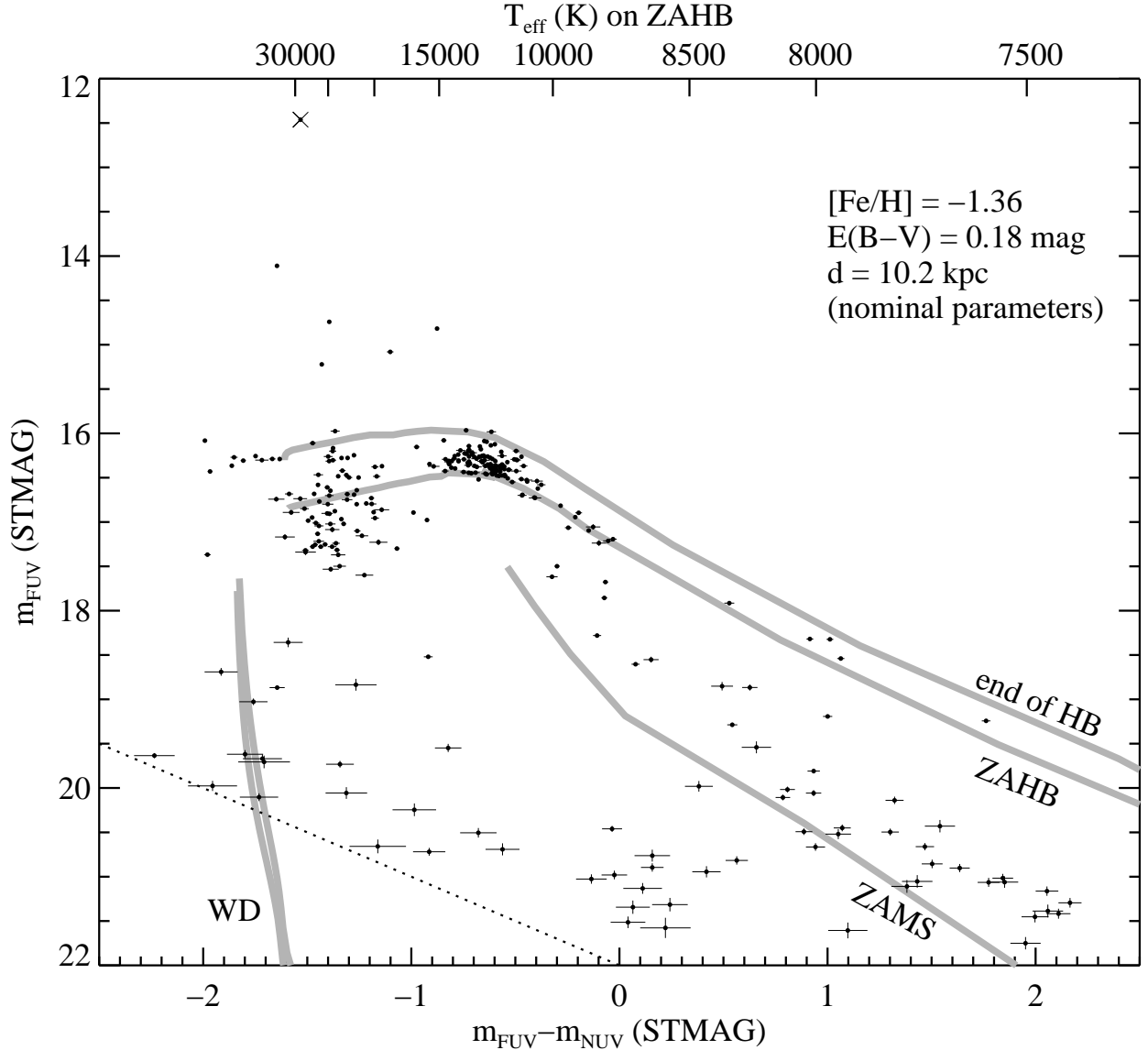


FIG. 3— The STIS UV CMD for NGC 2808. The different stages of stellar evolution are traced by grey curves that were transformed to the observational plane assuming the nominal cluster parameters. The exposure depth is variable across the image, so the photometric errors do not uniformly increase in size toward fainter magnitudes, but all stars on or near the HB are well-detected. The lower bound of the HB locus is the zero-age HB, and the upper bound is the point where the star has completed 99% of its core He-burning lifetime. One post-AGB star appears in the CMD (X), and was also observed spectroscopically by STIS (see Figure 2). The locus of BHB stars falls within the theoretical boundaries, but the EHB stars spread well below the ZAHB. Five stars that lie ~ 1 mag above the EHB fall in the expected location for post-HB stars. The BS sequence falls near an extension of the ZAMS (labeled; Bertelli et al. 1994), truncated at $1.7 M_{\odot}$. A faint WD sequence is also detected (labeled; Wood 1995). The dotted line represents the catalog limit at $m_{FUV} = m_{NUV} = 22$ mag.

spectroscopy (see Figure 2). The other five stars are post-EHB stars; their position in the CMD agrees well with the slowest phase of AGB-Manqué evolution, which has a lifetime that is ~ 5 times shorter than the HB lifetime. Thus, there should be ~ 5 EHB stars for every post-EHB star, in good agreement with the number of stars within the canonical EHB locus. Note that a few of these 29 stars might be the post-HB progeny of the sub-luminous EHB stars, instead of normal EHB stars. However, the number of post-EHB stars is considerably smaller than expected if one assumes they are the progeny of the entire EHB population (75 stars). Interestingly, in NGC 6752, Landsman et al. (1996) found only four post-EHB stars descended from a population of 63 apparently normal EHB stars.

There is also a string of 9 stars at $16 < m_{FUV} < 16.5$ mag and $-2 < m_{FUV} - m_{NUV} < -1.6$ mag that lie hotter and brighter

than the hot end of the HB. These stars are too hot and faint to be normal AGB-Manqué stars. Indeed, the bluest of these 9 stars have colors that would imply temperatures well over 100,000 K, depending upon the spectra used for the color transformation. Strong emission lines (e.g., C IV $\lambda 1550 \text{ \AA}$) could provide enough flux in the narrow far-UV bandpass to significantly shift the color towards the blue, but we have no reason to expect such emission in hot HB or post-HB stars. The stars are also too numerous to be hot WDs, else we would see far more stars along the WD cooling curve. Cataclysmic variables (CVs) with strong C IV and He II emission in the far-UV have been found in the globular cluster 47 Tuc (Knigge et al. 2000), but CVs are much too faint and cool to provide a viable explanation.

The most intriguing possibility is that these 9 hot stars may

be the AGB-Manqué progeny of the subluminoous EHB stars. Indeed, theoretical lifetimes predict that there should be ~ 9 such post-HB stars for the 46 subluminoous EHB stars. We will briefly return to this possibility in §8.3, after we discuss the origin of the subluminoous EHB stars.

Although the post-HB stars are interesting for further study, we are concerned in the present work with two specific peculiarities of the HB in NGC 2808: the subluminoous EHB stars in our UV CMD, and the EHB gap in previous optical CMDs. These features are not predicted by theoretical fiducials based upon canonical stellar evolution theory, model atmospheres, and synthetic spectra. Thus, in §4, we explore in greater detail both the canonical HB evolution and the new evolutionary paths associated with high RGB mass loss (the flash-mixing scenario). This will drive the calculation of model atmospheres and synthetic spectra with abundance enhancements and departures from LTE, discussed in §5. In the subsequent sections, we will return to the observations and consider alternative explanations for these unusual features of the HB morphology in NGC 2808.

4. HORIZONTAL BRANCH EVOLUTION

4.1. Sequence Parameters

A major goal of this paper is to determine if the “flash-mixing” scenario outlined in §1 can account for the hot subluminoous stars and the EHB gap in NGC 2808. To explore this possibility, we have constructed a detailed grid of evolutionary sequences that follow the evolution of appropriate low-mass stellar models from the ZAMS through the HB phase and, in many cases, through the subsequent post-HB phases to the WD cooling curve. Most importantly, these calculations follow the evolution continuously through the helium flash to the ZAHB. As a result, we are able to investigate the conditions under which mixing between the core and envelope might occur during the helium flash. In contrast, standard calculations skip the helium flash entirely, due to its numerical complexity, and assume that the only effects of the helium flash are to remove the degeneracy of the helium core and to increase the carbon abundance in the core to a few percent by mass (see Sweigart 1994a). Thus canonical ZAHB models implicitly assume that the helium flash has no effect on either the envelope mass or composition.

All of our sequences had an initial helium abundance (Y) of 0.23 and a scaled-solar heavy-element abundance (Z) of 0.0015. During the first dredge-up along the lower RGB, the envelope helium abundance increased to 0.244. As demonstrated by Chieffi, Straniero, & Salaris (1991) and Salaris, Chieffi, & Straniero (1993) for the MS and RGB phases, and additionally by VandenBerg et al. (2000) for the HB phase, scaled-solar models can closely mimic models with an enhancement of the α elements, provided the total Z is the same and the models are not too metal-rich. For an α -element enhancement of $[\alpha/\text{Fe}] = 0.3$, as is appropriate for metal-poor globular-cluster stars (Carney 1996), this choice for Z corresponds to $[\text{Fe}/\text{H}] = -1.31$, a value within the range of the metallicity determinations for NGC 2808.

All of our sequences also started with the same main sequence mass M of $0.862 M_{\odot}$. This choice for the mass, together with our adopted composition, implies an age at the tip of the RGB of 13 Gyr. VandenBerg (2000) has derived a somewhat younger age of 11 Gyr for NGC 2808 from isochrone fitting to the optical CMD after using the theoretical ZAHB luminosity

to set the distance modulus. Such a modest reduction in the cluster age would, however, have no effect on the evolutionary behavior to be described below.

Our sequences differ from each other only in the amount of mass loss along the RGB, which we parameterized with the Reimers (1975, 1977) mass-loss formulation:

$$\dot{M} = -4 \times 10^{-13} \eta_R L / g R \quad (M_{\odot} \text{ yr}^{-1}),$$

where L , g , and R are the stellar luminosity, gravity, and radius, respectively, in solar units, and η_R is the well-known Reimers mass-loss parameter. We considered values of η_R from 0.0 (no mass loss) to 1.0. This range in η_R covers the evolution of stars that ignite helium while on the RGB to those that ignite helium at high effective temperatures on the WD cooling curve. For our largest values of η_R , the models fail to ignite helium, and instead evolve down the cooling curve as helium WDs. Mass loss was terminated in our calculations once the models evolved off the RGB by 0.1 in $\log T_{\text{eff}}$. At this point the convective envelope contained $\sim 0.0003 M_{\odot}$ while the total envelope mass was $\sim 0.003 M_{\odot}$.

In the following subsections, we will describe the evolution of these sequences in more detail, and will demonstrate that models that ignite helium on the WD cooling curve will undergo substantial flash-induced mixing between the helium core and the hydrogen envelope, thereby leading to a natural dichotomy in the subsequent EHB evolution. The implications of this flash mixing for the properties of the hottest EHB stars, the so-called blue-hook stars, will then be explored in the theoretical plane. We will also show that models without flash mixing cannot account for the subluminoous EHB stars in NGC 2808 or ω Cen.

4.2. Evolution to the Zero-Age Horizontal Branch

Figure 4 illustrates the various paths taken by our sequences during their evolution from the MS to the ZAHB. We define the ZAHB locus in this figure as the location of our models once the convective core has stabilized at the beginning of the central He-burning phase. The red end of the ZAHB is set by the model with $\eta_R = 0.0$.

For $\eta_R \lesssim 0.740$, the models remain tightly bound to the RGB until the helium flash. A typical example of such evolution is shown by the track for $\eta_R = 0.620$ (Figure 4a). Following helium ignition, this model rapidly evolved over $\sim 2 \times 10^6$ yr from the tip of the RGB to a ZAHB position on the BHB. The track in Figure 4b, for $\eta_R = 0.740$, represents the transition between sequences that ignite helium on the RGB and those that ignite helium after evolving off the RGB to high effective temperatures. In this case, mass loss on the RGB reduced the envelope mass to $0.03 M_{\odot}$, and the model arrived on the ZAHB at an effective temperature of 20,000 K, i.e., just at the boundary between the BHB and EHB.

Castellani & Castellani (1993) first showed that stars that evolve off the RGB due to high mass loss can still undergo the helium flash. This result was further explored by D’Cruz et al. (1996), who demonstrated that a post-RGB helium flash is possible over a rather large range in η_R ($\Delta\eta_R \sim 0.2$). Two examples of such post-RGB flashes are given in Figures 4c and 4d for $\eta_R = 0.800$ and 0.817, respectively. The $\eta_R = 0.800$ sequence ignited helium at a high luminosity as it was evolving across the theoretical HR diagram, while the $\eta_R = 0.817$ sequence ignited helium just after it reached the top of the WD cooling curve. This latter sequence then evolved to the hot end of the EHB at an effective temperature of 31,500 K. As we shall see, 0.817 is the largest value of η_R for which the models evolved to the

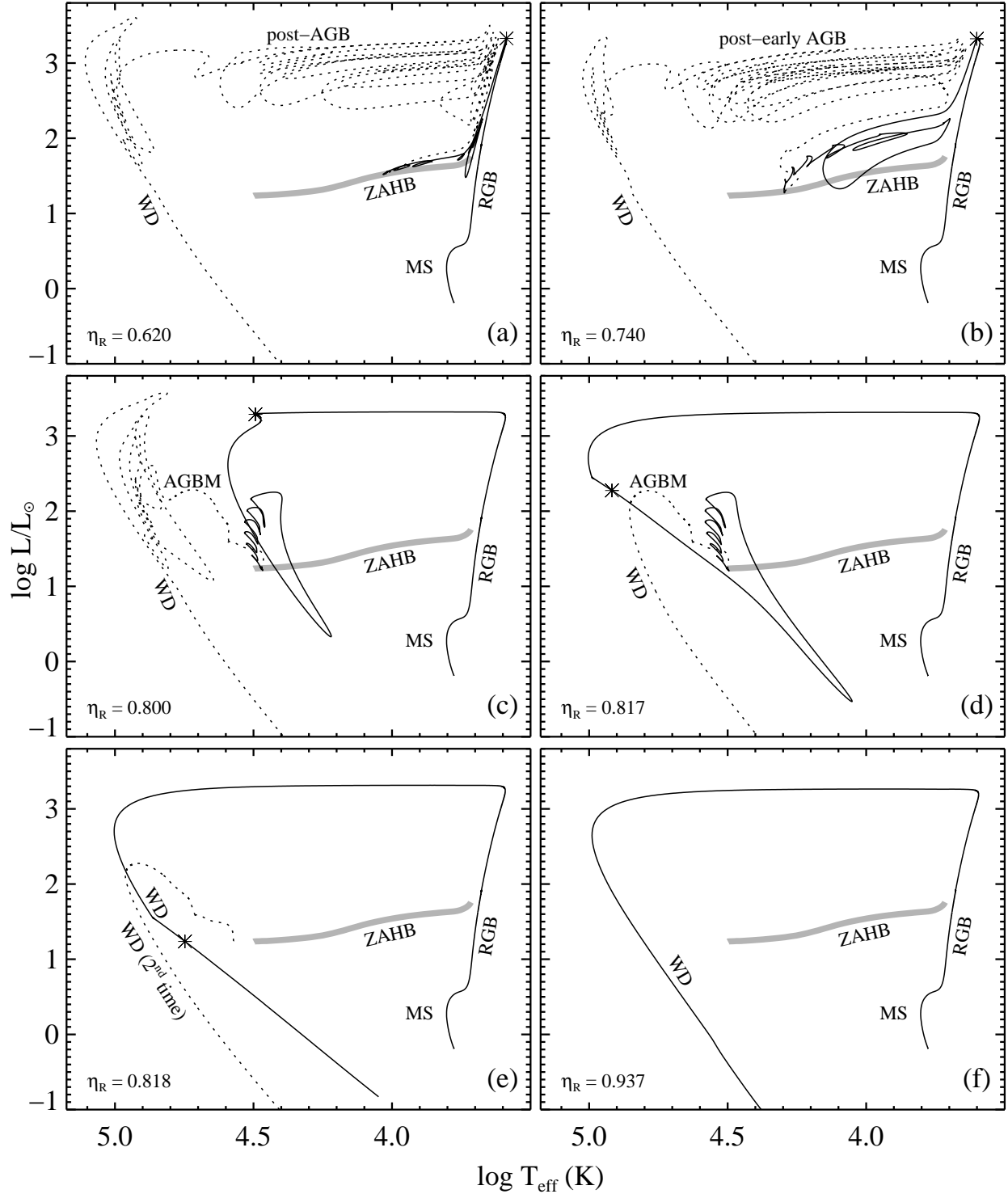


FIG. 4— Evolutionary tracks for selected values of the Reimers mass-loss parameter η_R . The evolution was followed continuously through the MS, RGB, and helium-flash phases to the ZAHB (solid lines) and then through the HB and post-HB phases to the WD cooling curve (dotted lines). The post-HB tracks either return to the asymptotic-giant branch (AGB; panels *a*, *b*) or evolve through an AGB-Manqué phase (panels *c*, *d*, *e*) before descending the WD cooling curve. The gyrations in the post-HB tracks are due to helium- and hydrogen-shell flashes. As η_R increases, the peak of the main helium-core flash (asterisk) shifts to higher temperatures, and the subsequent ZAHB location becomes hotter. The highest value of η_R that avoided flash mixing was $\eta_R = 0.817$ (panel *d*). The track for $\eta_R = 0.818$ ends when the flash convection penetrated into the hydrogen envelope (panel *e*). The subsequent evolution of this track is represented by a He + C blue-hook sequence. At $\eta_R > 0.936$ the star will not core-flash at all (e.g., panel *f*).

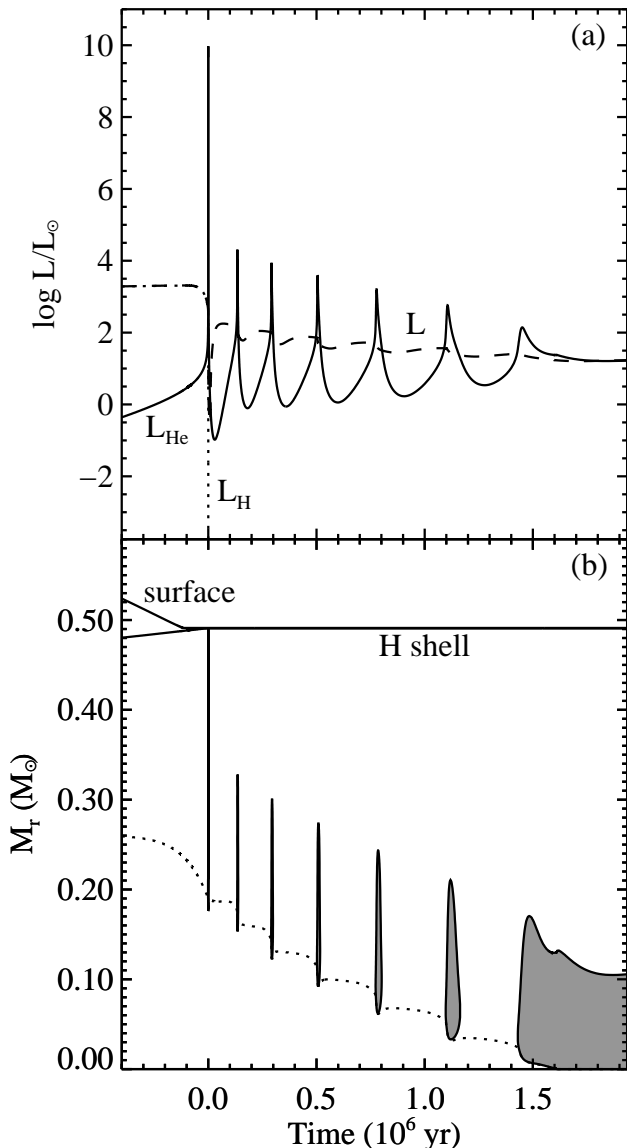


FIG. 5— Variation of the interior structure during the evolution through the helium-core flash to the ZAHB for the sequence with a Reimers mass-loss parameter $\eta_R = 0.817$. The zero-point of the timescale corresponds to the peak of the main flash. Panel *a* gives the time dependence of the helium-burning luminosity (solid curve), the hydrogen-burning luminosity (dotted curve), and the surface luminosity (dashed curve). Panel *b* gives the location in mass coordinate M_r of the flash-convection zones (shaded), the center of the hydrogen shell (labeled), and the stellar surface (labeled). The dotted curve in panel *b* shows the location of the temperature maximum within the core. Note that the main flash occurs off-center at $M_r = 0.18 M_\odot$. The main flash-convection zone failed to reach the hydrogen envelope by ~ 1 pressure-scale height. The evolutionary track for this sequence is plotted in Figure 4*d*.

ZAHB without flash-induced mixing between the core and the envelope.

In order to understand better the evolutionary behavior shown in Figure 4, as well as the conditions required for flash mixing, we need to look more closely at the structural changes that occur during the helium flash. We illustrate these changes for the $\eta_R = 0.817$ sequence in Figure 5. This sequence was chosen because the changes in its interior structure are typical

of those for smaller values of η_R and, most importantly, because it lies at the transition between the sequences with and without flash mixing. During the main helium-flash at time $t = 0$ in Figure 5*a*, the He-burning luminosity reached $9.4 \times 10^9 L_\odot$, and the e-folding time of the thermal instability dropped to only ~ 1 day. For 740 yr, the He-burning luminosity exceeded the surface luminosity (L) that was present during the previous evolution across the HR diagram ($\log L/L_\odot \sim 3.3$). The main flash was then followed by a series of lower-amplitude secondary flashes, as the He burning moved inward towards the center. These secondary flashes are responsible for the track gyrations that immediately precede the ZAHB phase in Figure 4. Eventually the He burning stabilized, and the star settled onto the ZAHB at $t = 1.94 \times 10^6$ yr.

One might expect the large amount of energy released during the main flash ($\sim 1.5 \times 10^{49}$ erg) to produce a sudden increase in the surface luminosity. However, virtually all of this energy goes into lifting the degenerate core out of its deep potential well. In fact, energy actually flows inward from the inner part of the envelope into the core just after the main flash peak. So, even though the star produces an enormous amount of energy in its deep interior during the main flash, very little of this energy actually reaches the surface.

The expansion of the core during the main flash cools the hydrogen shell, thereby causing the hydrogen-burning luminosity (L_{H}) to drop abruptly at $t = 0$ in Figure 5*a*. The star then faces an energy crisis, because it has lost the primary energy source for supplying its surface luminosity. The only available energy source comes from the gravitational contraction of the star's envelope. The drop in the surface luminosity following the main flash peak in panels *a* to *d* of Figure 4 coincides with this envelope contraction, as the star struggles to fulfill its energy needs. This luminosity drop becomes more pronounced with increasing η_R , because the envelope mass is then smaller. The time required for the surface luminosity to drop from its value at the main flash peak in Figure 4 to its subsequent minimum is very short, only ~ 8000 yr for the $\eta_R = 0.817$ sequence.

The convection zones produced by the main and secondary flashes during the $\eta_R = 0.817$ sequence are shown in Figure 5*b*. Due to neutrino cooling of the central part of the core during the preceding RGB phase, the maximum temperature within the core is located off-center, and consequently the main helium flash occurs in a shell at the mass coordinate $M_r = 0.18 M_\odot$. The high outward flux during the main flash sets up a temporary convection zone that extends from the flash site out to a point just inside the hydrogen shell. This convection zone lasts for only 3,400 yr and is therefore not resolved in Figure 5*b*. An expanded view of the outer edge of this convection zone during its closest approach to the hydrogen shell is presented in Figure 6. Note that the flash convection fails to reach the inner edge of the hydrogen shell by $\sim 10^{-3} M_\odot$ or, equivalently, ~ 1 pressure-scale height, and hence flash mixing does not occur in this case. Similar results were found for all of our sequences with $\eta_R \leq 0.817$.

While the main flash removes the degeneracy of the layers outside the flash site, the layers inside the flash site remain degenerate. This is simply a consequence of the fact that very little energy flows into these layers over the short timescale of the main flash. The subsequent secondary flashes then peel off successive layers from this inner degenerate core, until the temperature maximum and the He burning reach the center and the star forms a central convective core. At this point the star has arrived on the ZAHB.

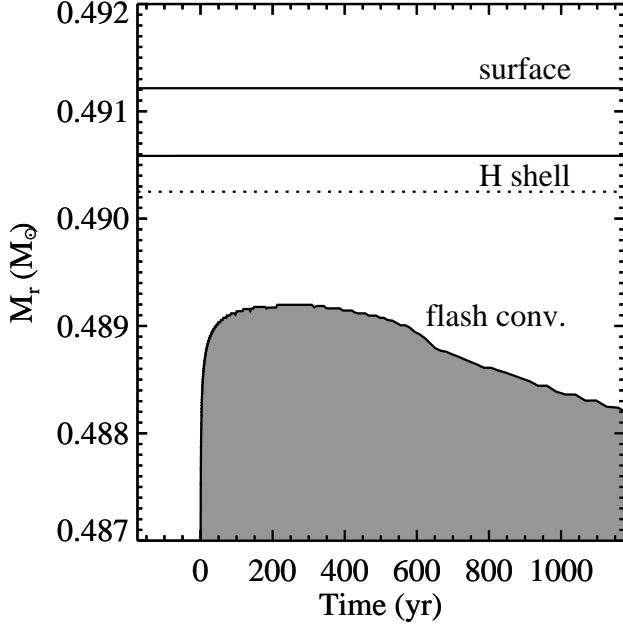


FIG. 6— Time dependence of the mass coordinate M_r at the outer edge of the flash-convection zone, the center of the hydrogen shell, and the stellar surface during the main helium flash shown in Figure 5. The dotted line denotes the inner edge of the hydrogen shell where $X = 10^{-6}$. The zero-point of the timescale corresponds to the peak of the main helium flash. Shaded areas are convective.

We conclude that flash mixing does not occur if a star ignites helium either on the RGB or during the evolution to the top of the WD cooling curve. In these cases our results confirm the canonical assumption that the helium flash does not change the envelope mass or composition.

4.3. Flash Mixing on the White Dwarf Cooling Curve

The above evolution changes dramatically when the helium flash occurs further down the WD cooling curve, as first noted by Sweigart (1997). Figure 4e shows the evolutionary track for a sequence where the helium flash did not begin until $\log L/L_\odot \approx 1.7$. Following the peak of the main flash at $\log L/L_\odot \approx 1.2$, the surface luminosity dropped rapidly for 30 yr, until at $\log L/L_\odot \approx -0.8$ the flash-convection zone reached the hydrogen shell and began to mix protons from the envelope into the hot He-burning interior. At this point the model calculations were stopped because of the numerical difficulties discussed below. The same flash mixing was found for all of our sequences with $0.818 \leq \eta_R \leq 0.936$. Sequences with $\eta_R \geq 0.937$ failed to ignite helium and consequently died as helium WDs. An example of this latter evolution is given in Figure 4f.

We emphasize the sharpness of the dichotomy between the “canonical” evolution for $\eta_R \leq 0.817$ and the “flash-mixing” evolution for $0.818 \leq \eta_R \leq 0.936$. Even though the difference in η_R between the sequences in Figures 4d and 4e is only 0.001, corresponding to a difference in mass loss of only $10^{-4}M_\odot$, the helium-flash evolution of these two sequences is strikingly different. In §6.2 and §7 we will argue that this dichotomy is responsible for both the hot subluminal stars and the EHB gap in NGC 2808.

The reason for this dichotomy in the helium-flash evolution can be straightforwardly explained. What fundamentally distinguishes the canonical sequences from the flash-mixing sequences is the strength of the hydrogen shell at the time of

the helium flash. As shown by Iben (1976) in the context of the helium-shell flashes, the high entropy of a strong hydrogen-burning shell acts as a barrier preventing the outward penetration of the flash convection into the hydrogen envelope. This is the case for all of our sequences with $\eta_R \leq 0.817$. However, the size of this entropy barrier decreases as a star descends the WD cooling curve and its hydrogen shell weakens. Beyond some point, bracketed by the $\eta_R = 0.817$ and 0.818 sequences in Figure 4, flash mixing becomes possible. Because flash mixing is a consequence of the basic properties of the stellar models, we conclude that such mixing should be a general characteristic of any star that ignites helium on the WD cooling curve.

The mixing found in our helium-core flash sequences is remarkably similar to the mixing that occurs during a very late helium-shell flash on the WD cooling curve, according to the “born-again” scenario for the origin of the hydrogen-deficient stars (e.g., Iben et al. 1983; Iben 1984, 1995; Renzini 1990). In both cases, the flash-convection zone is only able to penetrate into the hydrogen envelope once the hydrogen shell has been partially extinguished. The ingestion of the envelope hydrogen by the convection zone during a very late helium-shell flash leads to s-process nucleosynthesis and possibly Li production via the Cameron-Fowler mechanism (Herwig & Langer 2001; Herwig 2001b). In addition, C is dredged up from the deep, He-burning interior. The H-deficient, C-rich surface composition resulting from such mixing supports the “born-again” interpretation of the R CrB stars, the central stars of planetary nebulae of Wolf-Rayet spectral type (WC), and the PG 1159 stars (Blöcker 2001; Herwig 2001c). Further support comes from the rapid evolution and abundance changes observed in the stars FG Sge and Sakurai’s object. Both of these stars have undergone substantial hydrogen-depletion and s-process enrichment, and both seem to be presently evolving into R CrB stars (Gonzalez et al. 1998; Asplund et al. 1999). Thus the observational evidence for flash-induced mixing on the WD cooling curve seems very strong (Renzini 1990; Iben 1995).

The theoretical models currently available for the born-again scenario provide a helpful guide for predicting the effects of flash mixing during the helium-core flash. Here we will summarize the main events that should follow the onset of flash mixing in our evolutionary sequences. As protons from the envelope are mixed inward through the flash-convection zone, they will be carried into regions of higher temperature and will begin to react with the ^{12}C nuclei produced by the He burning (Herwig 2001c). Because the number of protons in the envelopes of our flash-mixing sequences is less than the number of ^{12}C nuclei in the flash-convection zone, these proton-capture reactions will lead primarily to the production of ^{13}C through the reactions $^{12}\text{C}(p,\gamma)^{13}\text{N}(\beta^+\nu)^{13}\text{C}$ (Sanders 1967). The peak of these reactions will occur around the layer in the flash-convection zone where the proton-capture timescale for ^{12}C becomes comparable to the mixing timescale. Assuming that all of the envelope hydrogen in our flash-mixing models ($5 \times 10^{-4}M_\odot$) is captured by the flash-convection zone, we find that the energy released by this proton burning will total $\sim 3 \times 10^{48}$ ergs, corresponding to $\sim 20\%$ of the energy released by the main helium-flash. Thus the burning of the envelope hydrogen will create a substantial, if only temporary, new energy source for the star.

Two important consequences follow from the development of this new energy source. First, the flash-convection zone will split into two distinct convection zones separated by a thin radiative region, i.e., an outer zone powered by proton burning

at its base and an inner zone powered by He burning. Such splitting of the flash-convection zone has been found during helium-shell flashes by Sweigart (1974) and Caloi (1990). As a result, ^{13}C production will be largely confined to the outer convection zone. Second, the energy input into the envelope from the proton burning should expand the star back to giant-branch dimensions, possibly leading to the formation of a convective envelope and further dredge-up. Following the consumption of the envelope hydrogen, these two convection zones will again coalesce into a single convection zone. At this point, ^{13}C from the outer zone will be carried into the hotter He-burning layers, where s-process nucleosynthesis via the reaction $^{13}\text{C}(\alpha, n)^{16}\text{O}$ can then occur.

The detailed investigation of the flash-mixing phase poses a formidable numerical challenge, in large part because the proton-capture reactions within the flash-convection zone occur on a timescale that is similar to the convective mixing timescale. Thus one has to solve for the nucleosynthesis and the time-dependent convective mixing simultaneously. In the only available calculation to follow the evolution of a globular-cluster star through the helium flash with flash mixing, Sweigart (1997) demonstrated that the flash-convection zone will penetrate deeply into the hydrogen envelope. In this case, the subsequent ZAHB model had an envelope hydrogen abundance X of 0.15, a helium abundance Y of 0.81, and a carbon abundance of 0.03 by mass. These calculations did not, however, include the energy from the proton burning, and therefore should underestimate the extent of the surface composition changes. Until recently, all calculations for very late helium-shell flashes in post-AGB stars likewise omitted the energy from the proton burning (e.g., Iben et al. 1983; Iben 1984). The one exception was the work of Iben & MacDonald (1995). To overcome this limitation, Herwig et al. (1999) and Herwig (2001a) have developed a new diffusion algorithm for coupling the nucleosynthesis to the convective mixing, and have successfully applied their algorithm to the problem of mixing during a very late helium-shell flash. Their results, as well as those of Iben & MacDonald (1995), show that flash-induced mixing will strongly deplete the envelope hydrogen abundance. It would be especially interesting to apply this technique to the case of a helium-core flash, although the numerics would probably be more demanding, due to the higher burning rates and shorter evolutionary timescale.

In view of the above numerical difficulties, we terminated our sequences as soon as they encountered flash mixing. Nevertheless, we can still predict the surface composition that these sequences should have when they arrive on the ZAHB. The calculations discussed above clearly indicate that flash mixing will consume most, if not all, of the envelope hydrogen. Thus we expect the surface composition of the flash-mixing models to be strongly depleted in hydrogen and enriched in helium. The surface carbon abundance should be close to its value in the flash-convection zone, namely, 0.04 by mass. In addition, an enhancement of the s-process elements, as seen in FG Sge and Sakurai’s object, would also be expected.

In the following subsection, we will explore the impact of these composition changes on the HB evolution and, more specifically, will show that these changes will lead to a dichotomy in the ZAHB effective temperature. Both the differences in the surface composition and the ZAHB effective temperature will prove important for understanding the properties of the blue-hook stars. We will also contrast our “flash-mixing” models with models that ignore the effects of flash mixing.

4.4. Blue-Hook Models with Hydrogen-Depleted Envelopes

As explained above, there is a clear distinction between our sequences with $\eta_R \leq 0.817$ and those with $0.818 \leq \eta_R \leq 0.936$. For $\eta_R \leq 0.817$, the models undergo the helium flash prior to descending the WD cooling curve and, as a result, evolve to the canonical ZAHB without any flash-induced mixing between the helium core and hydrogen envelope. In contrast, the models for $0.818 \leq \eta_R \leq 0.936$ do not ignite helium until they are on the WD cooling curve. Under such circumstances the flash-convection zone is able to penetrate deeply into the envelope, thereby greatly modifying the envelope mass and composition. As will be seen below, the models with flash mixing form a “blue-hook” feature near the hot end of the EHB as they begin their HB evolution. Such a feature is evident in the CMD of ω Cen reported by D’Cruz et al. (2000). In §6.2 we will identify both these blue-hook stars in ω Cen and the hot subluminal stars in NGC 2808 with our EHB models that undergo flash-mixing. For these reasons we will refer to our EHB models with flash mixing as “blue-hook” models in the following discussion. This will also serve to differentiate them from the canonical EHB models without flash mixing.

Some properties of our sequences with $\eta_R \geq 0.60$, corresponding to ZAHB $T_{\text{eff}} \gtrsim 10,000$ K, are presented in Figures 7 and 8. As indicated in Figure 7, the canonical EHB and blue-hook regions are populated over a rather large range in η_R , from 0.740 to 0.936. As mentioned earlier, this result agrees well with the results of D’Cruz et al. (1996), who found that EHB models could be produced over a similarly large range ($\Delta\eta_R \sim 0.2$) for both metal-poor and metal-rich compositions. Note that the EHB models of D’Cruz et al. (1996) include both the canonical EHB and blue-hook models in Figure 7. The lower panel of Figure 7 shows, however, that only models within the narrow range from $0.780 \leq \eta_R \leq 0.817$ ignite helium while evolving from the tip of the RGB to high effective temperatures. Most of the hot ZAHB models in the top panel of Figure 7 ignite helium either as they are just peeling off the RGB ($0.740 \leq \eta_R \leq 0.780$) or as they are descending the WD cooling curve ($0.818 \leq \eta_R \leq 0.936$). Indeed, the blue-hook models span $\sim 60\%$ of the range in η_R producing ZAHB models hotter than 20,000 K. Given a uniform distribution in η_R , we would therefore expect somewhat more than half of the “hot He-flashers” discussed by D’Cruz et al. (1996) to undergo flash mixing. This is also evident in Figure 1 of D’Cruz et al. (1996), where many of the hot He-flashers lie on the WD cooling curve at helium ignition.

The variation in the total mass (M), core mass (M_c), and envelope mass (M_{env}) with η_R is shown in Figure 8 for our BHB, EHB, and blue-hook models. The total mass decreases linearly with η_R until the models begin to peel away from the RGB prior to helium ignition. The change in slope at $\eta_R \approx 0.79$ is a consequence of turning off the Reimers mass-loss in the calculations after the models leave the RGB. As expected, the core mass is virtually constant at $M_c = 0.491 M_\odot$ for $\eta_R \leq 0.817$, but then decreases by $\sim 0.01 M_\odot$ for the blue-hook models. In the next subsection, we will demonstrate that such a modest decrease in M_c cannot (by itself) explain the subluminal stars in NGC 2808 and ω Cen. While one might expect the envelope mass to decrease monotonically with η_R , this is not, in fact, the case. The bottom panel of Figure 8 shows that M_{env} reaches a lower limit of $\sim 6 \times 10^{-4} M_\odot$ for all of the blue-hook models. The same behavior is also found in Table 1 of D’Cruz et al. (1996), where the minimum M_{env} decreases

from $\sim 2 \times 10^{-3} M_{\odot}$ at $[\text{Fe}/\text{H}] = -2.26$ to $\sim 8 \times 10^{-4} M_{\odot}$ at $[\text{Fe}/\text{H}] = 0.37$. This result implies that canonical ZAHB models cannot be extended to arbitrarily small M_{env} in order to match the hottest observed HB stars, as has sometimes been assumed (see, e.g., Sosin et al. 1997). We will show below that the composition changes associated with flash-mixing of the envelope naturally create hotter stars, thus alleviating the need for very small envelope masses.

As discussed previously, our blue-hook sequences were not evolved completely through the helium-flash phase, due to the numerical difficulties associated with the flash mixing, and consequently we had to adopt a different procedure for computing the blue-hook ZAHB models. We proceeded in two steps. Starting with the canonical ZAHB model for $\eta_R = 0.817$, we first adjusted the values of M_c and M_{env} until they matched the values for the blue-hook models plotted in Figure 8. A similar procedure is often used to compute canonical ZAHB models with different envelope masses. Next we changed the envelope composition of the models. Because detailed calculations including the energetics are not yet available for the flash-mixing phase, we decided to construct three sets of blue-hook models in order to explore the effects of different envelope compositions. The first set (hereafter He+C models) had an enhanced helium abundance of 0.96 and a carbon abundance of 0.04 by mass, with the remaining heavy elements having their initial cluster abundances. As noted above, such a composition reflects the composition of the flash-convection zone and is therefore the most likely outcome of flash mixing. The second set

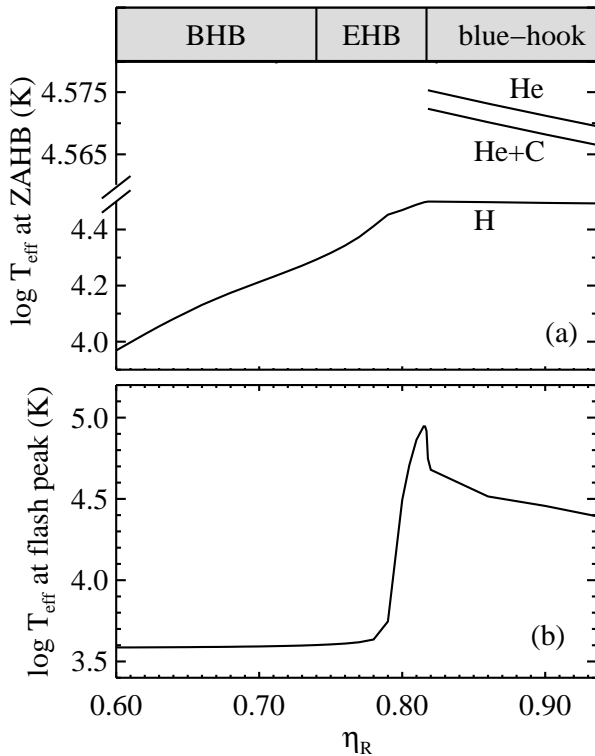


FIG. 7— Effective temperature at the ZAHB (panel *a*) and at the peak of the main helium flash (panel *b*) as a function of the Reimers mass-loss parameter η_R . At the top of the figure we indicate the ranges in η_R giving rise to the BHB, canonical EHB, and blue-hook models. The $\log T_{\text{eff}}$ scale changes at $\log T_{\text{eff}} = 4.50$ in panel *a* in order to show the differences in the predicted temperatures of the H, He, and He+C blue-hook models more clearly.

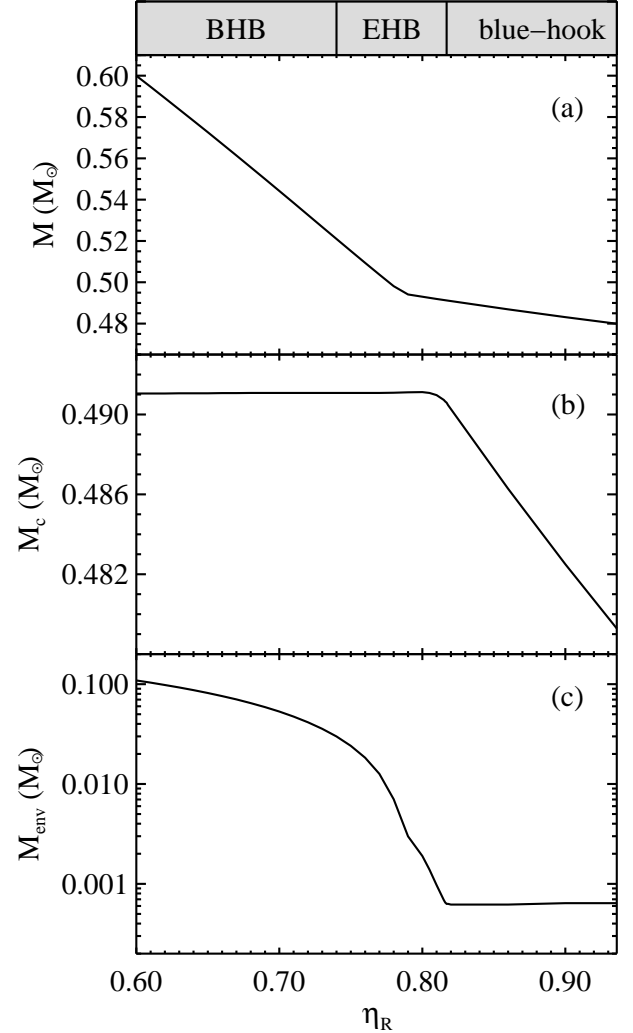


FIG. 8— Total mass M (panel *a*), core mass M_c (panel *b*), and envelope mass M_{env} (panel *c*) at the helium flash as a function of the Reimers mass-loss parameter η_R . At the top of the figure we indicate the ranges in η_R giving rise to the BHB, canonical EHB, and blue-hook models. The core mass is constant for $\eta_R \lesssim 0.80$ and then decreases by $\sim 0.01 M_{\odot}$ for the blue-hook models. Note that all of the models that ignite helium on the WD cooling curve have nearly the same envelope mass of $6 \times 10^{-4} M_{\odot}$.

(hereafter He models) had a pure helium envelope, except for the initial heavy-element abundance of 0.0015. With this set we could determine the effects of enhanced helium by itself. Finally the third set (hereafter H models) had the same hydrogen-rich envelope composition as the canonical EHB models. We computed this set to determine where blue-hook models without flash mixing would lie in a CMD. Discussion of these H blue-hook models will be postponed to the next subsection. All of these calculations were carried out for four values of η_R , namely, $\eta_R = 0.818, 0.860, 0.900$ and 0.936 . We then evolved all of these ZAHB models through the HB and post-HB phases.

The HB evolutionary tracks for each set of blue-hook models, together with some of our hottest canonical EHB tracks, are plotted in Figure 9. The rate of evolution along these tracks is indicated by the dots, which are separated by a time interval of 10^7 yr. Overall these tracks have the expected morphology, namely, they evolve upward in luminosity at an approximately constant T_{eff} .

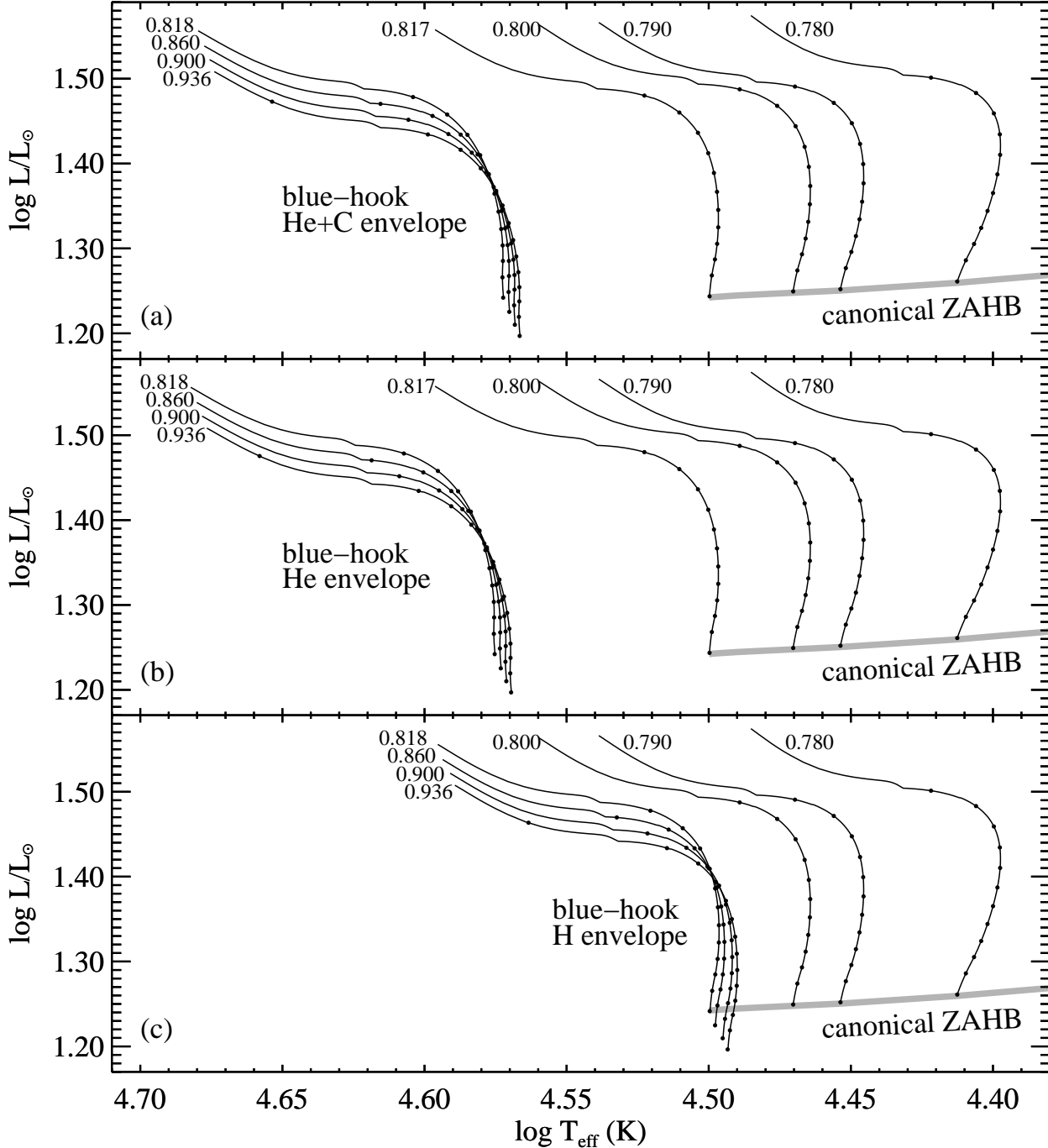


FIG. 9– HB evolutionary tracks for blue-hook sequences with He+C envelopes (panel *a*), He envelopes (panel *b*) and H envelopes (panel *c*). Each track is labeled by its value of η_R . For comparison, we plot the canonical HB tracks for $\eta_R = 0.780, 0.790, 0.800$, and 0.817 , as well as the canonical ZAHB (grey curves). The dots along each track are separated by a time interval of 10^7 yr. Note the dichotomy between the predicted effective temperatures for the He+C and He blue-hook tracks and the canonical tracks. In contrast, the H blue-hook tracks lie at the hot end of the canonical EHB.

Several features of the tracks in Figure 9 deserve comment. First, we note that there is a well-defined high temperature limit to the canonical EHB at $T_{\text{eff}} \approx 31,500$ K. Within the canonical framework, it is not possible to produce hotter EHB stars, because the envelope mass cannot be reduced below $6 \times 10^{-4} M_{\odot}$ for $Z = 0.0015$, regardless of the extent of mass loss along the RGB. In contrast, the blue-hook tracks with He+C or He envelopes form a distinct group located at a significantly higher effective temperature than the hot end of the canonical EHB. The properties of the blue-hook tracks within each group

depend only slightly on the value of η_R . They are also rather insensitive to the envelope carbon abundance, although some differences will be apparent when these tracks are transformed to the observational plane (see §6.2).

Figures 9*a* and 9*b* again illustrate the abruptness with which the tracks shift blueward with the onset of flash mixing (see also Figure 7*a*). Over an interval of only 0.001 in η_R , from 0.817 to 0.818, the predicted HB temperature jumps by ~ 6000 K, from $\approx 31,500$ K to $\approx 37,200$ K. For comparison, the same change in η_R near the hot end of the canonical EHB would produce

an increase in T_{eff} of only ~ 100 K. These results are consistent with the previous calculations of Sweigart (1997), who also found that his flash-mixing model did not lie at the hot end of the canonical EHB, but rather at a much higher effective temperature, closer to the domain of the high gravity He-sdO stars (Lemke et al. 1997). It is also interesting to note that the only known He-sdB star in a globular cluster (F2-2 in M15) has an effective temperature of 36,000 K (Moehler, Heber, & Durrell 1997), close to that predicted for our blue-hook models with flash mixing.

These features of the blue-hook tracks with He+C or He envelopes have some important implications. First, it is clear that flash mixing introduces a natural dichotomy in the properties of hot HB stars, which manifests itself as a gap centered at $T_{\text{eff}} \approx 34,400$ K in the theoretical temperature distribution. In §7 we will identify this flash-mixing gap with the high temperature gap observed within the EHB of NGC 2808. At first glance, there would appear to be a mismatch between this theoretical gap temperature and the temperature of $\sim 25,000$ K derived by fitting canonical ZAHB models to the optical CMD of NGC 2808 (Sosin et al. 1997; Bedin et al. 2000). However, this apparent mismatch can be largely attributed to HB evolution. Due to the temperature insensitivity of $B - V$ along the HB blue tail, the tracks in Figure 9 will evolve vertically towards brighter V magnitudes in the $(V, B - V)$ CMD. Thus the blue-hook tracks will appear to fill in the range in V magnitudes corresponding to the temperature range of the flash-mixing gap. At the same time, the hottest EHB models will also evolve towards brighter V magnitudes, thereby depleting the hot end of the canonical EHB. The net effect is to shift the apparent location of the EHB gap towards cooler temperatures than the actual gap in the stellar parameters. This point is discussed more fully in §7.

Due to their smaller core masses, the blue-hook ZAHB models in Figures 9a and 9b lie somewhat below the extension of the canonical ZAHB. However, these ZAHB models are only fainter by ~ 0.1 mag, whereas the hot subluminoous HB stars in NGC 2808 and ω Cen lie as much as ~ 0.7 mag below the ZAHB in the UV. In §5.2 and §6.2 we will show that the hydrogen-depleted surface compositions of the flash-mixing models will suppress the far-UV flux in the stellar spectra and thereby potentially explain the fainter luminosities of these sub-ZAHB stars. The higher effective temperatures of the He+C and He blue-hook models will also imply larger bolometric corrections, and hence fainter V magnitudes, for these models in an optical CMD. Thus, the blue-hook and canonical EHB models make different predictions concerning the faint end of the blue HB tail. These predictions will be tested against the observed faint end of the HB in NGC 2808 (Walker 1999; Bedin et al. 2000), once our models have been transformed to the observational plane.

4.5. Blue-Hook Models With Hydrogen-Rich Envelopes

We now consider the blue-hook models with hydrogen-rich envelopes plotted in Figure 9c. These models assume that flash mixing does not change either the envelope mass or composition, and therefore they represent, in effect, the continuation of the canonical EHB to higher mass-loss rates. We computed these H blue-hook models in order to study how hot HB models evolve when flash mixing is ignored, and to provide a set of hydrogen-rich models for comparison with the He+C and He blue-hook models.

The properties of the H blue-hook models differ significantly

in several respects from those of the He+C and He blue-hook models. We first note that all of the H blue-hook models in Figure 9c lie near the hot end of the canonical EHB, forming a hook-like feature that extends to slightly cooler temperatures and fainter luminosities. There is, however, no dichotomy in the predicted effective temperatures between the H blue-hook models and the canonical EHB models, and hence no obvious way to produce the EHB gap observed in NGC 2808. Moreover, there is no increase in the maximum EHB temperature beyond the hot end of the canonical EHB, and thus no increase in the length of the blue HB tail in the optical CMD. All of this is a consequence of the very similar envelope masses of the H blue-hook models and the hottest canonical EHB models. The fainter luminosities of the H blue-hook models are due entirely to the smaller core masses of these models. However, the maximum luminosity offset from the canonical ZAHB is only ~ 0.1 mag, much less than observed among the hot sub-ZAHB stars in NGC 2808 and ω Cen. This discrepancy cannot be explained by differences in the spectral energy distribution, because both the H blue-hook and canonical EHB have the same hydrogen-rich envelope composition.

The H blue-hook models in Figure 9c can be directly compared to the ‘‘hot He-flashers’’ of D’Cruz et al. (1996, 2000), which likewise do not include the effects of flash mixing. As can be seen in Figure 2 of D’Cruz et al. (1996), the hot He-flashers all lie at the hot end of the canonical EHB, with no indication of a gap in the temperature distribution between these models and the canonical EHB models. Again we find that the luminosities of the hot He-flashers are, at most, only ~ 0.1 mag fainter than the canonical ZAHB, due to the fact that the core masses of these models are only $\sim 0.015 M_{\odot}$ smaller than the canonical value. Overall the H blue-hook models and hot He-flashers agree very well.

The only way in which the H blue-hook models and the hot He-flashers can account for the faint sub-ZAHB stars in NGC 2808 and ω Cen is by reducing the mass of their helium cores. To examine this point more closely, we computed a series of HB sequences starting with a representative EHB model with $\eta_R = 0.780$. In these sequences, we reduced the core mass in increments of $0.01 M_{\odot}$ to a value $0.08 M_{\odot}$ smaller than the canonical value, while keeping the envelope mass constant at $0.007 M_{\odot}$. The results, shown in Figure 10, demonstrate that one would have to reduce M_c by $\sim 0.06 M_{\odot}$ in order to lower the ZAHB luminosity by 0.7 mag, as observed. The same conclusion can also be obtained from the HB sequences of Sweigart & Gross (1976). Such a large reduction in M_c is completely inconsistent with current evolutionary calculations (Sweigart 1994b). Even if such a reduction were possible, one would still face the quandary of understanding why only some stars had such small core masses.

We conclude that hot HB models with hydrogen-rich envelopes such as the present H blue-hook models or the hot He-flashers of D’Cruz et al. (1996) cannot explain the faint UV luminosities of the hot sub-ZAHB stars in NGC 2808 or ω Cen. In §6.2 we will show that such faint luminosities might be explained if the stellar envelope is hydrogen-deficient. The sub-ZAHB stars would then be fainter because of a difference in their spectral energy distribution, which suppresses the far-UV flux, as well as an increase in the bolometric correction.

5. MODEL ATMOSPHERES AND SYNTHETIC SPECTRA

To translate the stellar evolutionary models in §4 to the observational plane, we used several different sources of model

atmospheres and synthetic spectra, depending upon the type of star. It is extremely time-consuming and resource-intensive to compute new models, so we used existing grids of atmospheres and spectra where the accuracy of these older grids sufficed. New models were computed when an existing model could not accurately describe a given type of star. We discuss the models below.

5.1. Horizontal Branch Stars

For the canonical HB sequences, we used synthetic spectra at the cluster metallicity. These synthetic spectra were all calculated under the assumption of local thermodynamic equilibrium (LTE), which means that the distribution of atoms among their excitation and ionization states was calculated from the local values of two thermodynamic variables: temperature and electron density. At $\log g \leq 5.0$ (e.g., $T_{\text{eff}} < 20,000$ K on the ZAHB), we used the Kurucz (1993) grid of synthetic spectra, interpolating in T_{eff} and metallicity from the grid points that most closely matched each HB model. At HB surface gravities exceeding those available in the Kurucz (1993) grid, we used the ATLAS9 model atmosphere program (Kurucz 1993) to generate new LTE model atmospheres at the T_{eff} and surface gravity for each HB model, with metallicities bracketing the cluster metallicity (we can only run ATLAS9 at the discrete metallicity steps available in the published Kurucz grid). Note that most researchers simply use the Kurucz spectra at $\log g = 5$ to derive the colors of HB stars that exceed this gravity, and this practice is acceptable, because the change in surface gravity has only a small effect on the broad characteristics of the spectrum (the surface gravity on the ZAHB does not exceed $\log g = 6$). We generated these new atmospheres at higher gravities to ensure that a gravity mismatch on the EHB would not be the cause of any discrepancies between the data and stellar theory.

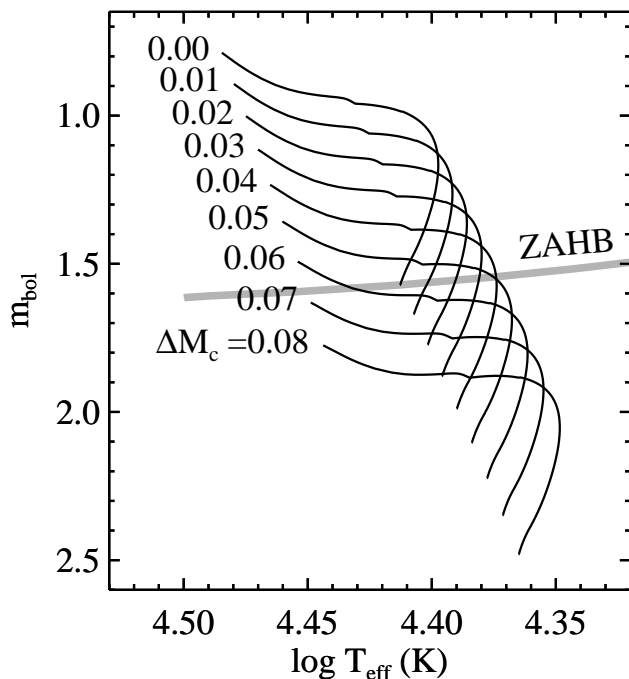


FIG. 10— Dependence of the bolometric magnitude along the HB evolutionary track of a representative EHB model on the mass of the helium core. The end of each track is labeled by the amount $\Delta M_c/M_\odot$ by which the core mass has been reduced below its canonical value. Note that an implausibly large decrease of $\Delta M_c \sim 0.06 M_\odot$ would be required to explain the luminosities of the hot sub-ZAHB stars in NGC 2808 and ω Cen.

We then used the SYNSPEC code (Hubeny et al. 1994) to create synthetic spectra from these model atmospheres, and the spectra were interpolated to give synthetic spectra at the cluster metallicity. Note that the agreement between the SYNSPEC spectra and the Kurucz spectra, where they meet at $\log g = 5$ on the HB, is excellent.

5.2. Blue-Hook Stars

Synthetic spectra with scaled solar abundances would not accurately represent the unusual stellar atmospheres present in blue-hook stars, because these stars should have greatly enhanced helium and carbon (see §4.4). The Kurucz (1993) grid assumes scaled-solar abundances, so we generated new model atmospheres with independently scaled abundances for the individual elements, using the TLUSTY model atmosphere code (Hubeny & Lanz 1995). We calculated atmospheres for each set of blue-hook models, using the three envelope compositions explained in §4.4 and displayed in Figure 9. The first composition set assumed enhanced helium (0.96 by mass) and enhanced carbon (0.04 by mass), with all other elements at the cluster abundance. The second set assumed enhanced helium (nearly 1.0 by mass) with heavier elements at the cluster abundance. The third set assumed scaled-solar abundances for all elements, with $[\text{Fe}/\text{H}] = -1.36$. We also computed two variations of the first set. One of these variations replaced the enhanced carbon with enhanced nitrogen, in case the carbon in the envelope was burned to nitrogen during the flash mixing and nucleosynthesis (although we note that there should not be enough protons in the envelope to do so). The other variation enhanced only the iron abundance, from the nominal cluster abundance, to a value of 1.25% by mass (i.e., 10 times the solar Fe mass fraction), to simulate the effects of radiative levitation on iron.

Hydrogen, helium, carbon, nitrogen, and iron were allowed to depart from LTE. About 550 individual levels of H, He, C, and N, and about 43,000 Fe levels, of the following ions, were included in the non-LTE TLUSTY model atmospheres: H I, He I, He II, C II, C III, C IV, N II, N III, N IV, N V, Fe III, Fe IV, Fe V, and Fe VI. These levels were grouped into about 400 superlevels. At the cluster abundance, the iron line-blanketing effect remains very small, and the atmosphere structure is significantly changed only when the iron abundance is strongly enhanced. Thus, we explicitly included the non-LTE treatment of Fe in our model atmospheres only when Fe was enhanced. When the atmosphere is carbon-rich, the details of the carbon opacity also become important, in particular strong and broad autoionization features appear in the far-UV spectrum. This opacity comes from the detailed cross-sections of the Opacity Project (Cunto et al. 1993), along with our use of the TLUSTY Opacity Sampling mode with small frequency steps.

Once we calculated the model atmospheres, we used the SYNSPEC code (Hubeny et al. 1994) to generate non-LTE synthetic spectra for each atmosphere. Species not included explicitly in the TLUSTY models were assumed to be in LTE. These spectra covered the range of 1,000–10,000 Å at 1 Å resolution, to allow computation of observed colors in various HST and ground-based bandpasses.

Our calculations show that blue-hook stars with flash-mixed atmospheres have significantly different spectra than stars at the cluster metallicity. We show the effects of these abundance enhancements in Figure 11. Note that for simplicity, this figure shows the emergent flux from the model atmospheres, and not the detailed synthetic spectra. In a normal stellar atmosphere composed mostly of hydrogen, the hydrogen opacity shortward

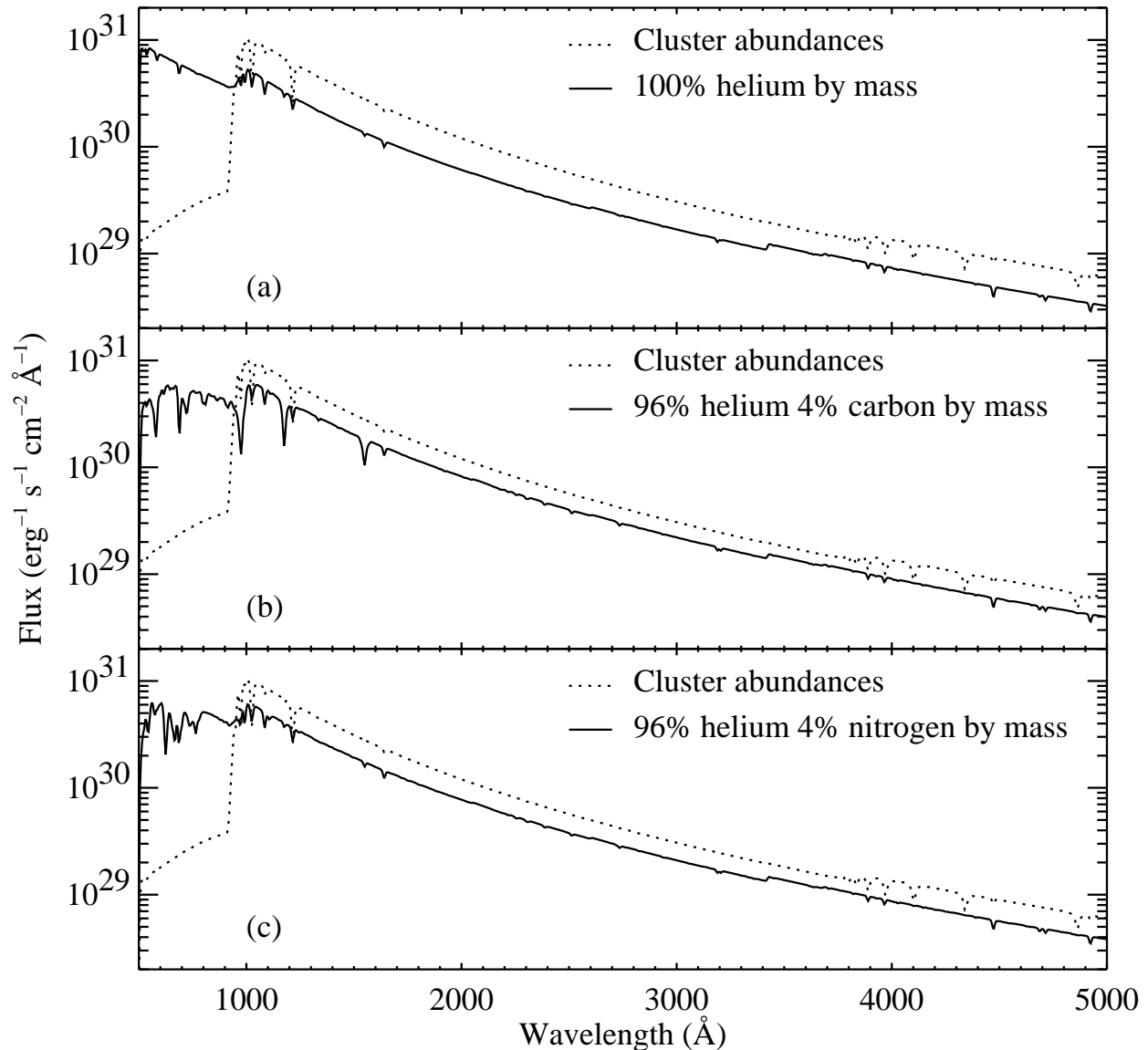


FIG. 11— Spectral energy distributions for a blue-hook star (solid curves) near $T_{\text{eff}} = 37,000$ K, for different assumed envelope compositions (see §4.4). In each panel, we show the emergent flux (not the detailed synthetic spectrum) on a log scale. The dashed line in each panel shows the flux from a canonical EHB atmosphere ($T_{\text{eff}} = 31,000$ K) that assumes the nominal cluster abundances. Panel *a* shows the flux from an atmosphere that is nearly 100% helium by mass; the reduction in hydrogen opacity increases the flux below 912 \AA , at the expense of flux at longer wavelengths. In panel *b*, increasing the carbon abundance restores some of the sub- 912 \AA opacity, and so the flux emerges at longer wavelengths. In panel *c*, we show that nitrogen could also provide this opacity, and thus the spectrum is similar to that with enhanced carbon.

of 912 \AA redistributes the flux in the extreme ultraviolet (EUV) to longer wavelengths. In an atmosphere with enhanced helium, the opacity below 912 \AA is greatly reduced, and so much more flux is radiated in the EUV at the expense of the flux at longer wavelengths. Enhancing the carbon abundance along with the helium restores some of this EUV opacity, but the resulting spectrum is still redder and fainter in the far-UV than that of a normal stellar atmosphere. Replacing carbon with nitrogen can also provide this EUV opacity.

6. NATURE OF SUBLUMINOUS EHB STARS

Having explored the theoretical implications of high mass loss on the RGB, we now return to the observations of NGC 2808 and its unusual HB morphology. Given our choice of distance modulus, the BHB stars at $T_{\text{eff}} < 15,000$ K in our STIS CMD (Figure 3) fall within the expected range of lumi-

nosities, while hotter stars begin to fall below the ZAHB. Note that this is not simply a translation of the entire HB population to fainter magnitudes: the EHB population has approximately twice the expected luminosity width in the far-UV. Thus, one needs to explain both the faint luminosities of the EHB stars and the EHB luminosity width in order to understand the STIS CMD.

As suggested in the preceding sections, the subluminous EHB stars in NGC 2808 may be the progeny of stars that underwent flash mixing on the WD cooling curve and that have arrived on the ZAHB with a greatly modified envelope composition. We will now examine this possibility in more detail, by translating the blue-hook models in §4.4 and §4.5 into the STIS CMD using the stellar atmospheres in §5.2. Before doing this, however, we will first rule out several alternative explanations involving photometric errors, larger reddening, and radiative levitation.

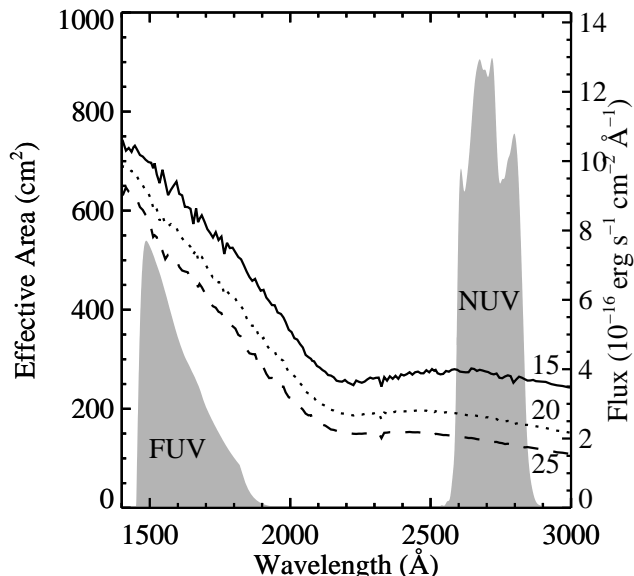


FIG. 12— Spectral energy distributions for stars at three different temperatures along the ZAHB: 15,000 K, 20,000 K, and 25,000 K (labeled). When compared to the STIS bandpasses (shaded curves), it is apparent that no calibration error could spread the EHB stars to fainter magnitudes, while not doing the same to the BHB stars. Also, the EHB stars should be as well-detected as the BHB stars, given the similar flux levels.

6.1. Alternative Explanations

6.1.1. Photometric Errors

The increased luminosity width on the EHB cannot be due to statistical errors in the photometry, because these errors are very small. We are not underestimating the size of these statistical errors on the EHB, because the luminosity width of the stars on the BHB falls within the expectations, and these stars are at approximately the same far-UV luminosity as the canonical EHB. One would not expect a change of one magnitude in the near-UV bandpass to dramatically increase the statistical scatter from < 0.1 mag to ~ 1 mag. Note that in these bandpasses, EHB spectra are not very different from BHB spectra (see Figure 12). In this figure, we show the theoretical spectra of three stars lying at different temperatures along the ZAHB. Because the shape and intensity of each spectrum is similar to the others, it is apparent that the statistical errors should not vary dramatically as one moves from $T_{\text{eff}} = 15,000$ K to $25,000$ K.

By similar reasoning, the increased luminosity width on the EHB cannot be due to systematic errors in the data. Both the EHB stars and the BHB stars are spread over the entire STIS image, and thus calibration problems (e.g., flat fielding errors, geometric distortion errors, focus changes, variability in exposure depth, hot pixels, dead pixels) should affect both classes of stars similarly. Furthermore, there is no change that can be made to the assumed sensitivity curves that would only depress the far-UV luminosity of some EHB stars while leaving other EHB stars and all BHB stars unchanged (see Figure 12), because these stars have similar spectra. In the same manner, no change in the assumed reddening law could depress some of the EHB stars relative to the other EHB stars and BHB stars.

6.1.2. Reddening

One might imagine that significantly increasing the assumed extinction could cause the theoretical EHB locus to drop off more sharply as a function of increasing temperature, which in

turn might increase the agreement with the STIS CMD, but this is not the case. As mentioned earlier, the foreground reddening and distance toward NGC 2808 are somewhat uncertain. Ferraro et al. (1990) compiled a list of $E(B - V)$ determinations for NGC 2808 from the literature, with the highest being well above the value reported in most studies: $E(B - V) = 0.34$ mag (Burstein & McDonald 1975). The spectra in Figure 12 demonstrate that it is difficult to depress the EHB relative to the BHB in the STIS UV bandpasses, because the EHB and BHB spectra have similar shape and intensity. Nevertheless, we demonstrate the effect of increased reddening in Figure 13. In this figure, we increased $E(B - V)$ to 0.34 mag while decreasing the distance, such that the BHB would still fall mostly within the theoretical HB locus. It is obvious that no choice of distance at this reddening will give agreement across the entire HB, and that increasing the reddening does not turn the HB significantly downward on the hot end. Moreover, the hottest EHB stars in Figure 13 lie blueward of the canonical EHB, and are thus unexplained.

Both Walker (1999) and Bedin et al. (2000) bring up the possibility of differential reddening toward this cluster, of ~ 0.02 mag. Differential reddening could increase the scatter in the STIS CMD, but then we would see increased scatter for both the BHB and EHB, not just the EHB. Furthermore, the change in m_{FUV} and m_{NUV} is only ~ 0.15 mag for a change in $E(B - V)$ of 0.02 mag, so it would take a very large differential reddening to reproduce the increased luminosity width seen on the EHB. Finally, the STIS field is much smaller than the ground-based fields, and so any differential reddening should be much smaller in the STIS photometry than in the ground-based photometry.

6.1.3. Radiative Levitation

Grundahl et al. (1999) have found photometric evidence that atmospheric diffusion plays an important role in HB morphology. That such processes may help explain HB anomalies was first suggested by Caloi (1999); later, spectroscopy of BHB stars by Behr et al. (1999), Behr, Cohen, & McCarthy (2000), and Moehler et al. (2000) confirmed that atmospheric diffusion can strongly affect BHB star abundances. In their CMDs of Galactic globular clusters with extended horizontal branches, Grundahl et al. (1999) found that BHB stars hotter than $\sim 11,500$ K are brighter in Strömgren u than predicted by canonical HB models (using cluster abundances), while the EHB and RHB stars agree with the models. They explain this jump in the u magnitude by invoking radiative levitation of heavy elements in stars spanning the range $11,500 \lesssim T_{\text{eff}} \lesssim 20,000$ K. This levitation greatly enhances the abundance of metals in the stellar atmosphere. The Grundahl et al. (1999) study showed that the effect on the CMD was strongly dependent upon the bandpasses used. At high atmospheric metallicity (up to $[\text{Fe}/\text{H}] = +1.0$), BHB stars become brighter (by $\lesssim 0.3$ mag) in Johnson U and Strömgren u , but become somewhat fainter (by $\lesssim 0.1$ mag) in WFC2/F160BW and UIT/1620 Å. Subsequent observations by Bedin et al. (2000) demonstrated that the same effect is present in the BHB of NGC 2808.

Our STIS far-UV bandpass is similar in wavelength coverage to the WFC2/F160BW bandpass studied by Grundahl et al. (1999), although it is far more sensitive. If atmospheric diffusion is affecting the abundances of the BHB stars only, one would expect a small depression of the BHB luminosity relative to that of the EHB and RHB stars, when in fact we see the opposite: a depression of the EHB luminosity relative to the

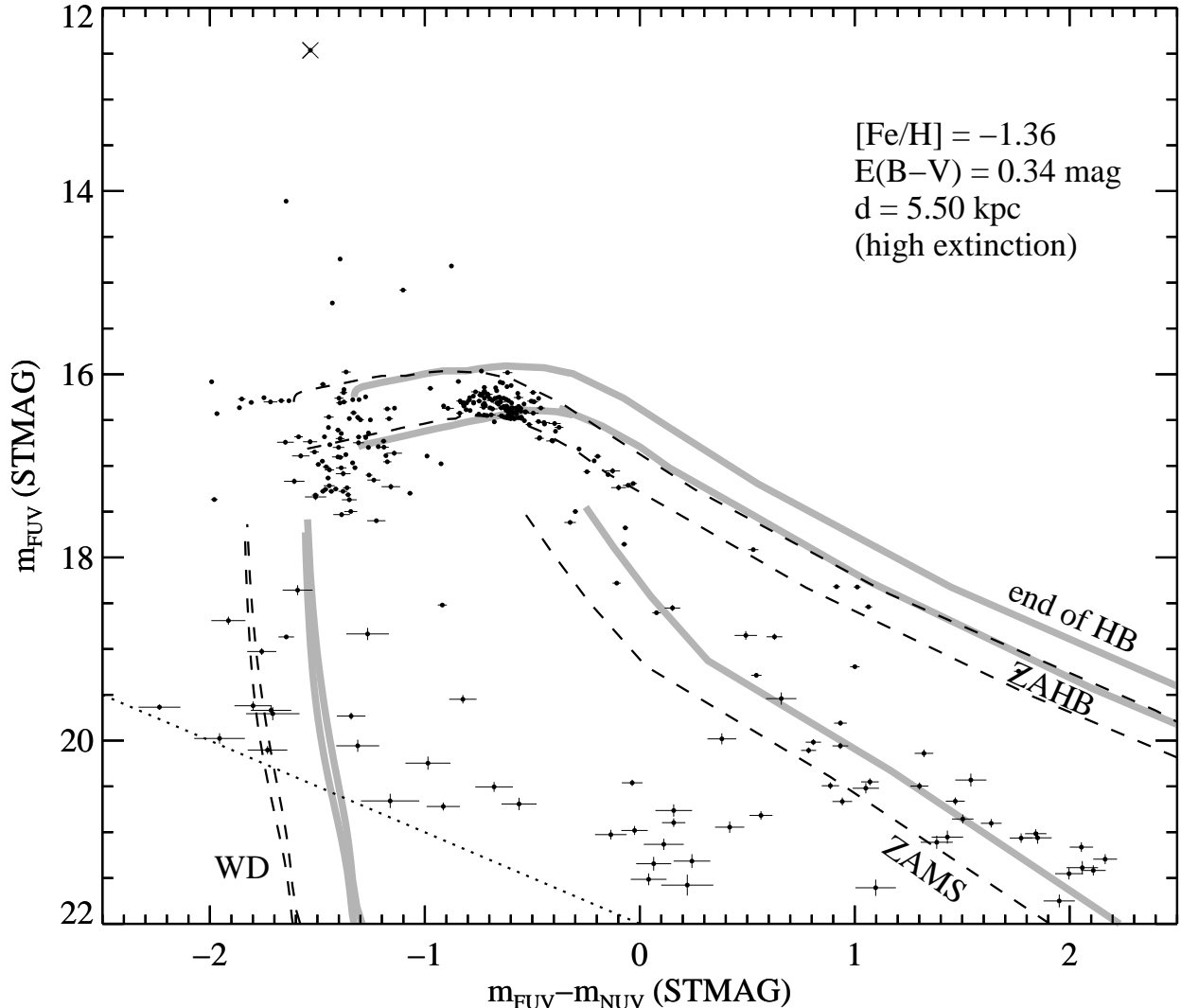


FIG. 13— Theoretical loci (grey curves) for the HB, ZAMS, and WD evolutionary phases in the same STIS CMD as shown in Figure 3. We translated the theoretical models to the observational plane while assuming a larger foreground reddening of $E(B-V) = 0.34$ mag. The distance modulus was set by matching the theoretical ZAHB to the lower boundary of the BHB stars. The dashed curves show the location of the theoretical loci when the nominal cluster parameters are assumed, as in Figure 3. This figure demonstrates that an increase in the assumed extinction cannot depress the EHB relative to the BHB.

BHB luminosity. Thus the Grundahl et al. (1999) results suggest that atmospheric diffusion does not explain the discrepancy seen in the STIS CMD of NGC 2808. Nonetheless, it is worth exploring the effect of enhanced atmospheric metallicity in our CMD. If, for some reason, our far-UV bandpass was to respond in the same manner as Strömgren u (which lies at longer wavelengths than the STIS far-UV bandpass), then the BHB stars would be brighter than expected, which would give the misleading impression that the EHB was too faint compared to the BHB. However, this would still not explain the unusually large EHB luminosity width.

To demonstrate the effect of atmospheric diffusion on our CMD, we translate the entire HB (regardless of T_{eff}) to the observational plane using synthetic spectra at $[\text{Fe}/\text{H}] = +1.0$ in Figure 14. The use of these models is meant to show the maximum effect of radiative levitation; our large metallicity enhancement is much higher than what is spectroscopically observed in BHB stars by Behr et al. (1999; 2000), in M13 and M15, and Moehler et al. (2000), in NGC 6752, where $[\text{Fe}/\text{H}]$ is

generally solar to a few times solar. For the range of temperature spanned by the BHB stars, a theoretical HB locus at solar metallicity (not shown in Figure 14) is very nearly coincident with the HB locus at the cluster metallicity (dashed), and thus the BHB stars in the STIS data appear at the expected luminosity for the likely range of atmospheric diffusion effects. Note that our use of scaled-solar models provides only an approximation to the effects of radiative levitation, because the light-element abundances generally do not show the strong abundance enhancements seen for iron. Figure 14 demonstrates that in the STIS bandpasses, HB stars become both fainter and redder at high atmospheric metallicity, regardless of T_{eff} ; i.e., the metallicity affects the far-UV band more strongly, so the translation is not simply downward in the CMD. It is clear from the figure that the BHB stars will not increase in luminosity if they are affected by atmospheric diffusion; they will decrease in far-UV luminosity, as expected.

What if diffusion is affecting the EHB stars more strongly than the BHB stars? In that case, the EHB stars would become

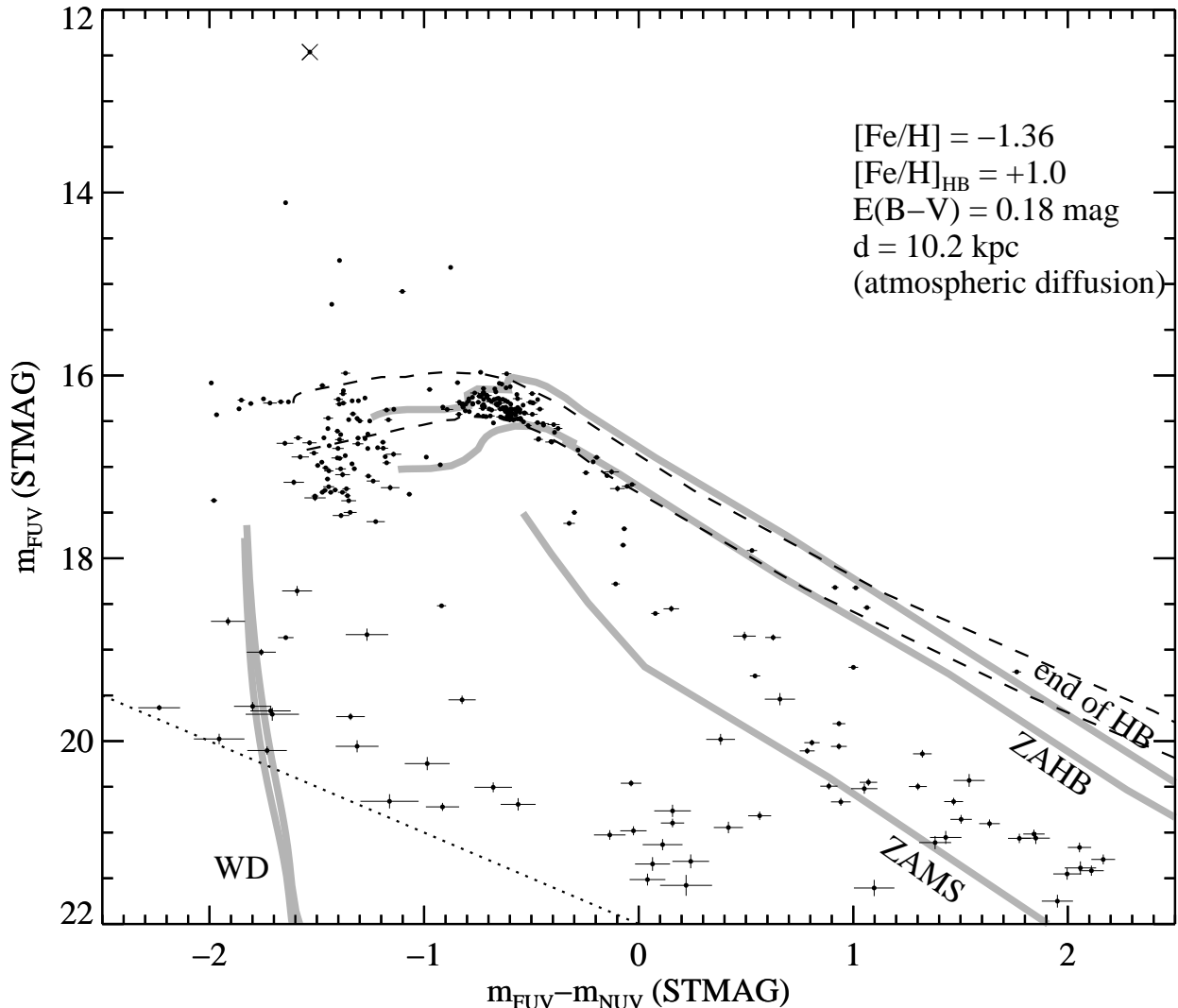


FIG. 14— The same STIS CMD shown in Figure 3, but with the entire theoretical HB translated to the observational plane (grey curves) while assuming an atmospheric abundance of $[\text{Fe}/\text{H}] = +1.0$ (note that atmospheric diffusion is only thought to affect HB stars at $11,500 \lesssim T_{\text{eff}} \lesssim 20,000 \text{ K}$). This metallicity-enhanced HB locus demonstrates that atmospheric diffusion cannot sufficiently depress the EHB relative to the BHB or increase the luminosity width of the EHB. The dashed curves show the location of the theoretical loci when the nominal cluster parameters are assumed, as in Figure 3.

fainter, relative to the BHB, but this would contradict the Grundahl et al. (1999) results, which show that the photometric effects of diffusion seem to be decreasing near $T_{\text{eff}} \sim 20,000 \text{ K}$. Furthermore, the EHB stars in the STIS CMD are not completely translated to fainter magnitudes; they are spread to fainter magnitudes, with an increased luminosity width. The only way to increase the far-UV luminosity width on the EHB is to assume a variable metallicity enhancement for the EHB stars. However, if one does this, the EHB stars in the data would still have a luminosity width that is larger than this ad hoc scenario. There is also no obvious way to account for the hottest EHB stars that lie blueward of the canonical EHB locus in Figure 14. In summary, atmospheric diffusion does not appear to explain the discrepancies between the data and the models.

6.2. Blue-hook Explanation

Blue-hook stars were the final explanation that we considered for the subluminous EHB stars in our CMD. These stars would coexist with the canonical EHB stars, instead of replac-

ing them, so they could potentially widen the apparent luminosity width of the EHB. To demonstrate where blue-hook stars would lie in the STIS CMD, we translated the ZAHB model of each $\eta_R = 0.860$ blue-hook sequence (see Figure 9) to the observational plane. As evident in Figure 9, the exact choice of η_R makes little difference, because all values of η_R within a composition set ($0.818 \leq \eta_R \leq 0.936$) have very similar tracks; we chose $\eta_R = 0.860$ simply because it is near the middle of the range.

Figure 15 shows the location of these ($\eta_R = 0.860$) blue-hook models in the STIS CMD. The circle shows the ZAHB model in the “H envelope” blue-hook track (see Figure 9 and §4.4), translated to the observational plane using a model atmosphere and synthetic spectrum with the nominal cluster abundance. Because the spectrum is dominated by hydrogen opacity, it is marked with an “H.” The square and diamond show, respectively, the ZAHB models for the “He envelope” and “H+C envelope” blue-hook tracks, translated to the observational plane with the appropriate atmospheres and spectra. The grey curve

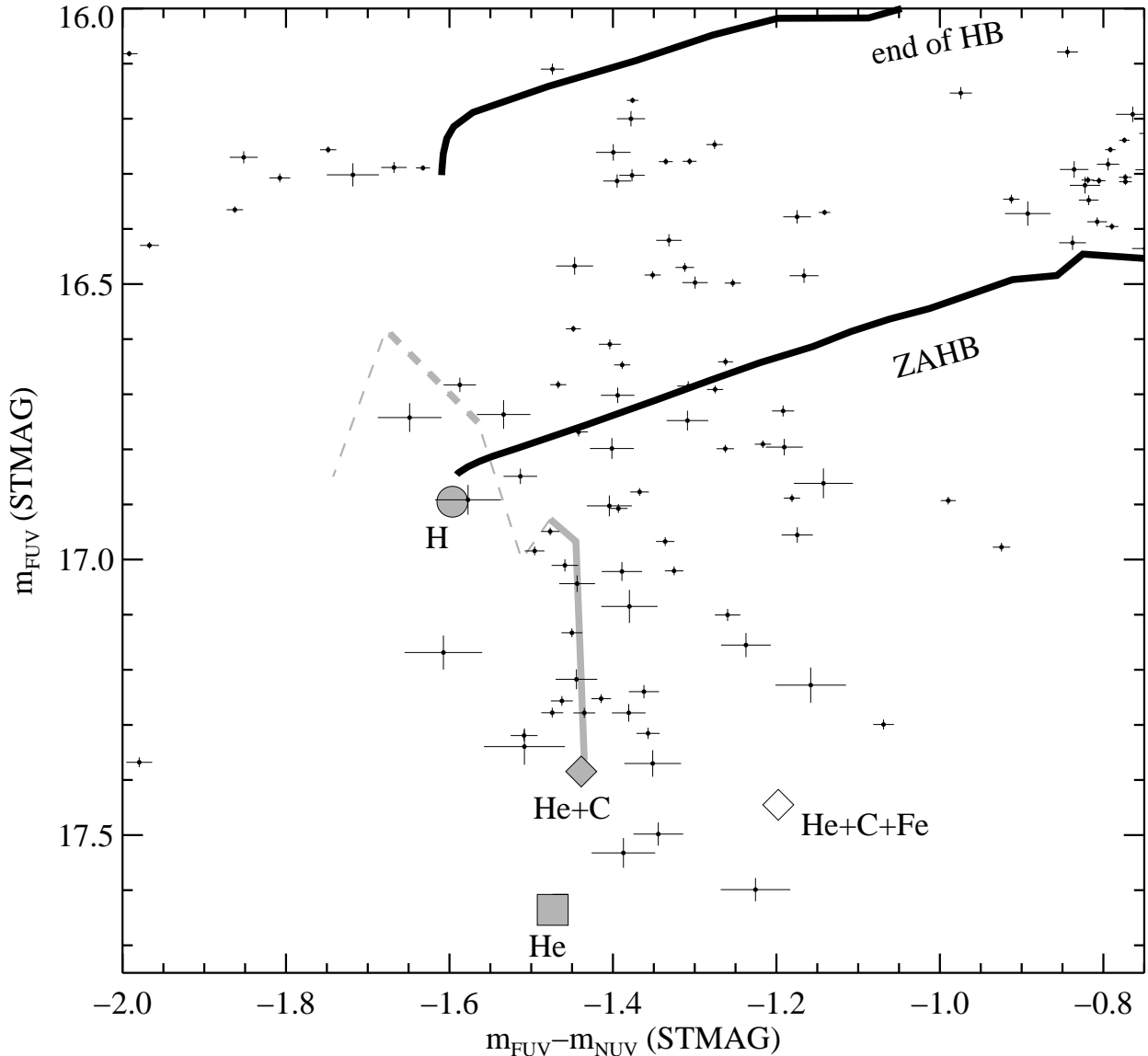


FIG. 15— Location of the $\eta_R = 0.860$ blue-hook ZAHB models in the STIS CMD. Blue-hook stars with normal H envelopes (circle) would begin their core He-burning evolution near the hot end of the canonical EHB, and thus do not explain the stars below the canonical ZAHB (labeled). Blue-hook stars with enhanced helium and carbon (diamond) atmospheres would begin their core He-burning evolution well below the canonical ZAHB, and then evolve to brighter luminosities (grey curve), filling in the area under the canonical ZAHB. If radiative levitation in the hot He+C models increased the iron abundance to $[\text{Fe}/\text{H}]=+1.0$, the models would become significantly redder (open diamond). The dashed grey curve shows the post-HB evolution of the He+C model, with thicker dashes denoting the slowest phase.

shows the HB evolution of the “He+C” model, with the post-HB evolution shown as a dashed line.

Figure 15 demonstrates that blue-hook stars with normal H envelopes cannot explain the subluminous stars in the STIS CMD: they are predicted to lie near the hot end of the canonical ZAHB. Looking at Figure 9, this is not surprising, because the H blue-hook sequences also lie near the canonical ZAHB in physical parameter space. The small ~ 0.1 mag drop in the far-UV luminosity comes from the small decrease in core mass, as discussed in §4 and also shown in D’Cruz et al. (1996, 2000). In contrast, the He and He+C models in Figure 15 show the same dramatic drop in far-UV luminosity that is present in the STIS data. Roughly half of the luminosity drop seen in the He and He+C models comes from the larger bolometric correction associated with their higher temperatures, as compared to the H blue-hook model; the rest of the luminosity drop and all of

the movement to the red comes from the effects of the envelope abundance changes on the emergent spectra. Thus, the location of blue-hook models in a CMD is very sensitive to the composition of the envelope and atmosphere, but not very sensitive to the reduced core mass. It is worth noting here that the distribution of metallicity in ω Cen might drive differences in its blue-hook morphology.

The blue-hook stars will evolve through their core He-burning phase in much the same way as canonical HB stars (see Figure 9): they will slowly evolve ~ 0.5 mag brighter in bolometric luminosity at roughly constant T_{eff} . They will then evolve more rapidly to hotter T_{eff} and brighter luminosities, and go through a phase very similar to the canonical AGB-Manqué evolution. Thus, the spread of stars in the STIS CMD between the blue-hook ZAHB (diamond) and the canonical ZAHB is due to the evolution of blue-hook stars to higher luminosities

(grey curve in Figure 15) as they undergo core He-burning. Together, the blue-hook and canonical stars would predict an EHB luminosity width very close to that observed in the STIS CMD.

Changes in the assumed atmospheric abundances could produce some scatter in the colors of the blue-hook stars. In §4.4, we found that the envelope of blue-hook stars would likely have greatly enhanced helium and carbon, and this corresponds to the “He+C” point in Figure 15. If the carbon abundance is not as high as 4% by mass, a blue-hook star will lie somewhere between the “He+C” point and “He” point. Although the supply of protons in the stellar envelope during flash mixing is not large enough to burn the carbon to nitrogen, replacing the enhanced carbon by enhanced nitrogen would move the He+C point (diamond) ~ 0.05 mag to the blue in Figure 15.

The colors of the blue-hook stars would also be affected by the radiative levitation of iron in the stellar atmosphere. For example, if the surface abundance of iron increased to $[\text{Fe}/\text{H}] = +1.0$, the $m_{FUV} - m_{NUV}$ color of a star at the same T_{eff} would be ~ 0.25 mag redder than the He+C point. This is shown by the open diamond in Figure 15, marked “He+C+Fe.” An enhanced iron abundance at the surface might also increase the stellar radius slightly, thus decreasing the T_{eff} , and this would also move the He+C point somewhat redder. The iron enhancement seen in BHB stars does not appear to be present in the cooler EHB stars (see §6.1.3; also see Bedin et al. 2000), but diffusion calculations (Charpinet et al. 1997) show that the surface iron abundance can be enhanced to solar or even super-solar abundances at $T_{\text{eff}} \gtrsim 30,000$ K, which is hotter than the canonical EHB but appropriate for blue-hook stars; these iron enhancements offer a possible driving mechanism for the pulsating sdB stars, which show solar iron abundances (Heber, Reid, & Werner 2000). Furthermore, it should be easier to enhance the iron abundance through radiative levitation if the atmosphere is mostly helium instead of hydrogen, because of the decrease in EUV opacity and the increase in the mean molecular weight in the atmosphere.

The blue-hook explanation of the subluminal EHB stars can be tested by comparing the location of the blue-hook models in different bandpasses with the observational data. For example, NGC 2808 was observed by Sosin et al. (1997) with WFPC2, using the F218W, F439W, and F555W bands. An examination of their figures shows a significant number of stars below the ZAHB, but the luminosity offset is somewhat smaller than in our STIS CMD. However, the F439W and F218W filters are not as sensitive to the anomalous abundances in flash-mixed blue-hook stars, as one might expect from an examination of Figure 11; as one moves from the far-UV to longer wavelengths, the He+C spectrum moves closer to the spectrum from a canonical EHB star. We further demonstrate this point in Figure 16, which shows the translation of the canonical ZAHB and blue-hook ZAHB models to the STIS bandpasses, the WFPC2 bandpasses, and ground-based bandpasses. Each panel in Figure 16 has the same range in color (1 mag) and luminosity (2 mags).

At a given color, the luminosity offset for the blue-hook models is smaller in the WFPC2/F439W bandpass than in the STIS/FUV bandpass. Also, in the WFPC2 CMD, He+C blue-hook stars should extend bluer than the hot end of the canonical ZAHB, while in the STIS CMD, these stars are redder than the hot end of the ZAHB. Thus, in the WFPC2 bandpasses, the He+C blue-hook stars would appear to lie near an extension of the canonical ZAHB, if it was drawn to arbitrarily small envelope masses and high T_{eff} . In fact, the theoretical ZAHB employed by Sosin et al. (1997) was extended

to $M_{\text{env}} = 10^{-4} M_{\odot}$ and $T_{\text{eff}} \approx 40,000$ K, which is far hotter than the true termination of the canonical ZAHB (see §4.2 and Figure 4). Note also that Sosin et al. (1997) transformed m_{F439W} to an approximate Johnson B , while we have retained the STMAG system for the WFPC2 bandpasses; for a synthetic spectrum at $T_{\text{eff}} = 25,000$ K, $\log g = 5$, and $[\text{Fe}/\text{H}] = -1.5$, $B = m_{F439W} + 0.66$ mag. Thus our models would appear to be approximately 0.7 mag fainter in B than in m_{F439W} . The predicted B magnitude of the He+C blue model in Figure 16b agrees well with the faint end of the EHB in the Sosin et al. (1997) ($m_{F218W} - B, B$) CMD.

Bedin et al. (2000) show a $(U - B, U)$ CMD of NGC 2808 in which the EHB stars are well-matched by an extension of the canonical ZAHB to very small envelope masses ($M_{\text{env}} = 4 \times 10^{-4} M_{\odot}$). In particular, there is no indication of subluminal stars in this CMD. This again demonstrates that the unusual nature of the blue-hook stars is most easily discerned in UV bandpasses. Comparison of the Bedin et al. (2000) CMD with Figure 16c shows excellent agreement: the blue-hook stars are predicted to lie directly along an extension of the hot EHB, just as observed. There is, however, a clear discrepancy between the faint end of the EHB at $U \sim 20.0$ mag in the Bedin et al. (2000) CMD and the faint end of the canonical ZAHB at $U \sim 19.4$ mag in Figure 16c. The fainter observed limit for the EHB is entirely consistent with the predicted U magnitudes of the blue-hook models. We note that this discrepancy is less pronounced in the Bedin et al. (2000) CMD because the canonical ZAHB plotted in this CMD extends to smaller M_{env} (and hence higher T_{eff}) than one would expect from the present calculations or the calculations of D’Cruz et al. (1996).

The $(B - V, V)$ CMD in Figure 16d also shows that the canonical ZAHB and the flash-mixed blue-hook models predict different limiting magnitudes for the faint end of the EHB. The canonical HB ends at $V \sim 20.4$ mag, while the blue-hook models extend another ~ 0.5 mag fainter to $V \sim 20.9$ mag. The deep photometry of Walker (1999) and Bedin et al. (2000) shows that the faint end of the blue HB tail in NGC 2808 is located at $V \sim 21.2$ mag, in good agreement with the predicted location of the blue-hook models, but not with the faint end of the canonical ZAHB. As noted in §4, there is no way within the canonical framework to extend the canonical ZAHB to fainter magnitudes. It appears, therefore, that canonical models cannot account for the extent of the blue HB tail in NGC 2808 in either the $(U - B, U)$ or $(B - V, V)$ CMDs.

In summary, the flash-mixed blue-hook models, when translated to the observational plane, are able to explain the luminosities of the faintest subluminal EHB stars, as well as the large luminosity width of the EHB in NGC 2808. Moreover, they are consistent with the locations of the hottest EHB stars in various observational bandpasses.

7. EHB GAP

There are three significant gaps in the NGC 2808 HB distribution. The gap between the BHB and RHB stars is stretched in the STIS bandpasses, and thus there are very few stars on the HB at $m_{FUV} - m_{NUV} > 0$ mag in Figure 3. At present, there is no plausible explanation for this strong bimodality of the HB distribution in NGC 2808. Sosin et al. (1997) reported two more gaps in the NGC 2808 HB distribution: one between the EHB and BHB stars, and one within the EHB itself. These gaps were confirmed in optical CMDs by Walker (1999) and Bedin et al. (2000). Our STIS CMD clearly shows the EHB-BHB gap, but the gap within the EHB is not present.

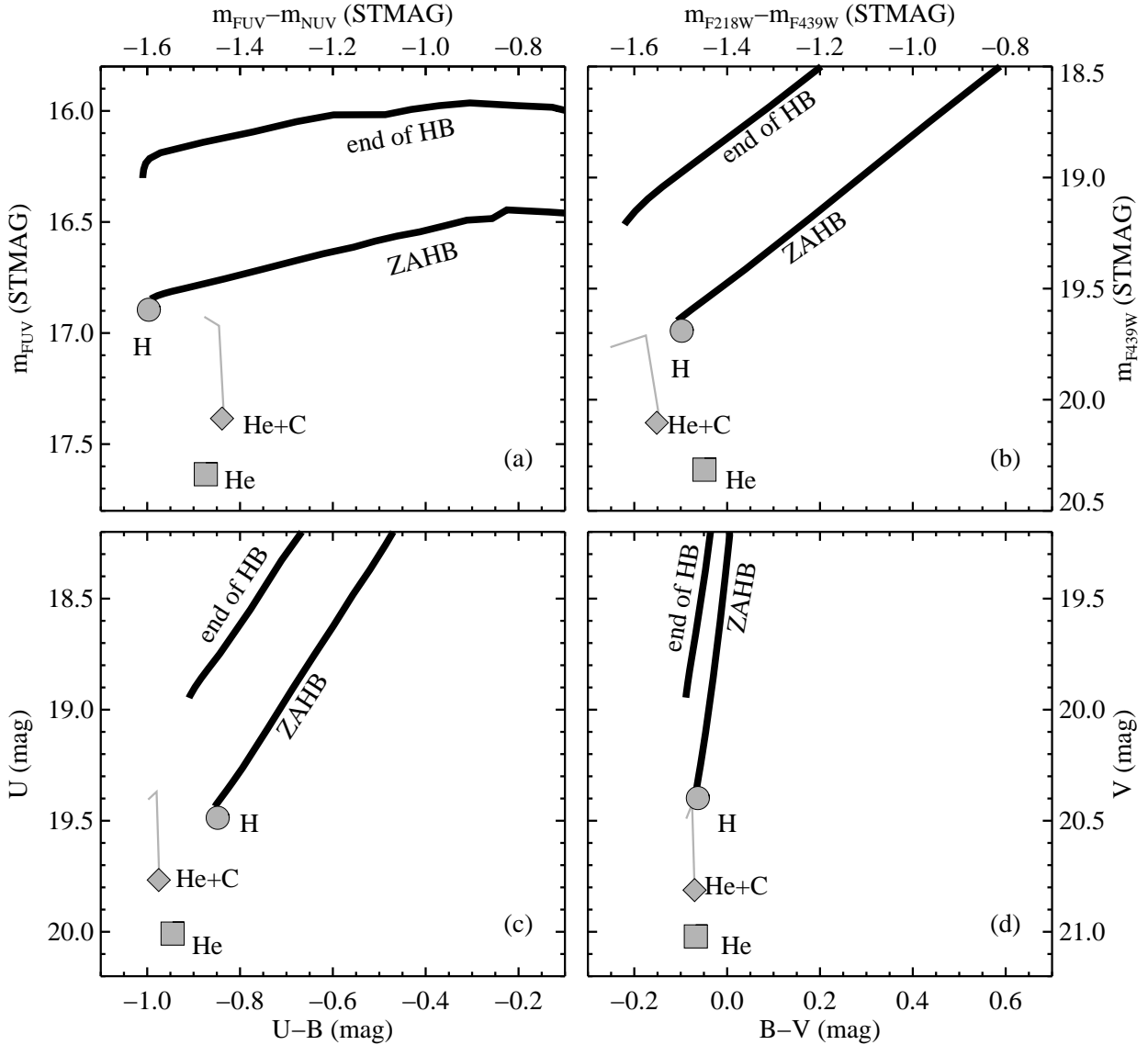


FIG. 16— Locations of the blue-hook ZAHB models and the canonical HB in four sets of bandpasses. The HB evolution of a blue-hook He+C model is shown as a grey curve, as in Figure 15. The stretch in color and luminosity is the same in each panel. Upper left: In the STIS bandpasses ($m_{FUV} - m_{NUV}, m_{FUV}$), the He+C blue-hook model lies fainter and redder than the hot end of the canonical ZAHB. Upper right: In the WFPC2 bandpasses ($m_{F218W} - m_{F439W}, m_{F439W}$), the He+C blue-hook model appears fainter and bluer than the end of the canonical ZAHB. Lower left: In a ground-based ($U - B, U$) CMD, the He+C model appears to lie along an extension of the canonical ZAHB. Lower right: in a ground-based ($B - V, V$) CMD, the EHB is nearly vertical, and again the He+C model appears to lie along an extension of the canonical ZAHB.

As noted in section §4.3, flash mixing should be a normal consequence of helium ignition on the WD cooling curve. In this section we will argue that the dichotomy produced by such mixing between the canonical EHB and blue-hook models is responsible for the EHB gap in the optical CMDs of NGC 2808. However, this possibility raises an important question: why are EHB gaps not apparent in the optical CMDs of other globular clusters with extended blue HB tails? For example, the optical CMDs of ω Cen reported by Kaluzny et al. (1997) and Lee et al. (1999) do not seem to show an EHB gap despite the substantial population of EHB stars. Quite possibly, any EHB gap in ω Cen has been blurred by the metallicity distribution in the cluster. Another candidate for an EHB gap is NGC 6273, which has one of the longest blue HB tails of any globular cluster (Piotto et al. 1999). Unfortunately, the CMD of NGC 6273 is affected by large differential reddening ($\Delta E(B - V) \sim 0.2$ mag; Piotto et al. 1999), which would likewise obscure any EHB gap. Other

globular clusters with long blue HB tails, e.g., M13, M80 and NGC 6752, do not contain a sufficient number of the faintest EHB stars ($M_V \gtrsim 4.5$ mag) to determine if an EHB gap is present (see, e.g., Figure 7 of Piotto et al. 1999). Thus NGC 2808 stands out as the globular cluster where an EHB gap is most easily detected observationally.

The absence of the EHB gap in the STIS CMD can be understood if one examines Figure 15. In the STIS bandpasses, the blue-hook models begin their core He-burning evolution redder and fainter than the canonical EHB, and then evolve to brighter luminosities (along the grey curve), filling in the area under the canonical ZAHB with “subluminous” HB stars. Thus one would not predict a gap in the STIS CMD once the HB evolution is taken into account. However, in the WFPC2 and ground-based bandpasses (Figure 16), the blue-hook models lie along an extension of the canonical ZAHB, separated by a gap in luminosity.

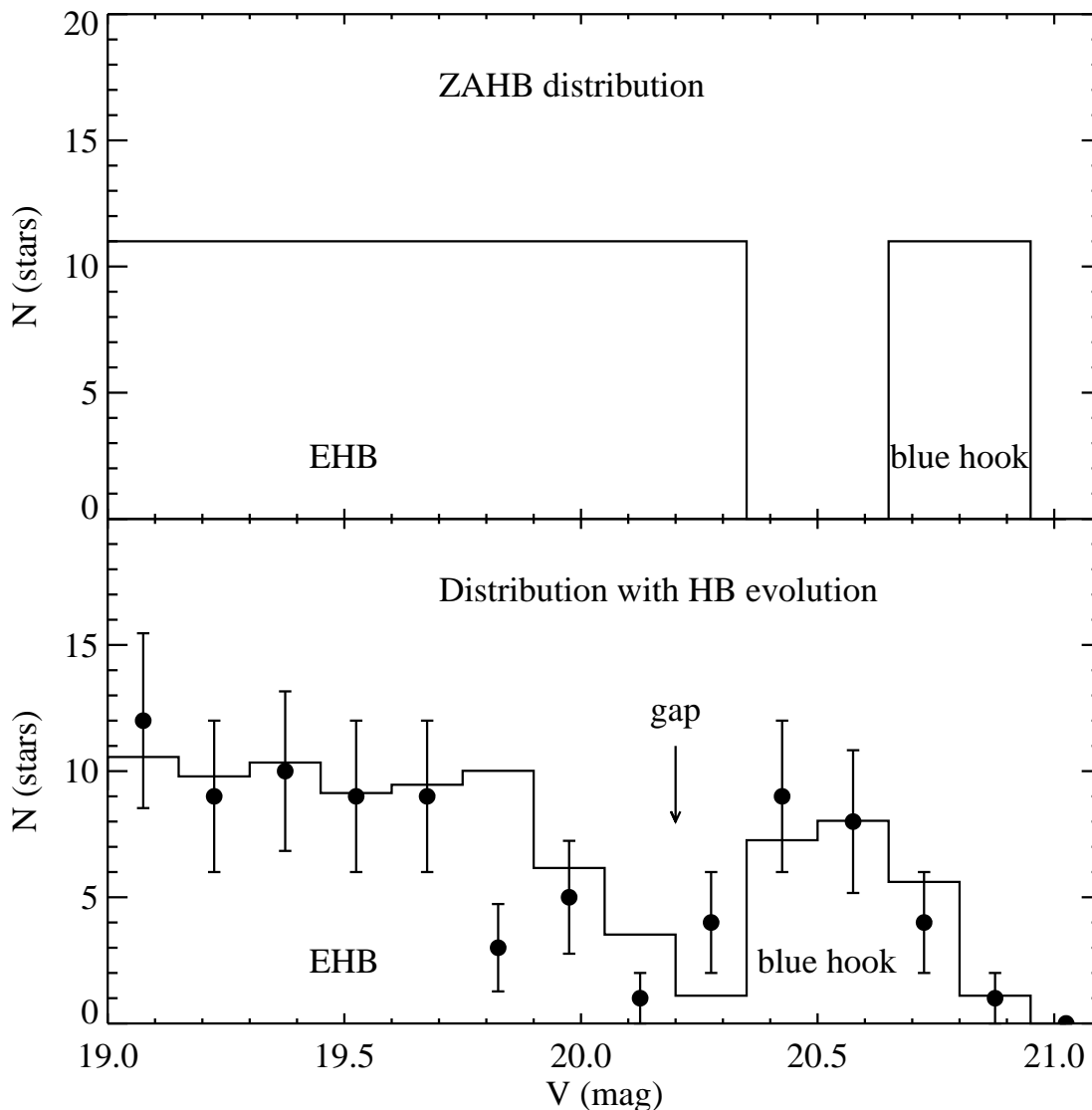


FIG. 17— Top panel: Assumed uniform distribution in V along the ZAHB, with a gap at $V \approx 20.5$ mag between the EHB and the He+C blue-hook stars (compare to Figure 16d). Bottom panel: Predicted distribution with HB evolution from the ZAHB distribution in the top panel. Note that the gap has shifted closer to $V \approx 20$ mag. For comparison, we plot the EHB luminosity function from Bedin et al. (2000) as points with their associated Poisson errors. The observed gap within the EHB coincides closely with the predicted gap between the EHB and blue-hook stars.

The EHB gap is very obvious in the $(B - V, V)$ CMD of NGC 2808 of Bedin et al. (2000) at $V \approx 20$ mag. Because the EHB is almost vertical in a $(B - V, V)$ CMD, they were able to use the luminosity function in V to analyze this gap, concluding that this gap is probably real and not a statistical fluctuation. The separation between the blue-hook models and the canonical EHB, shown in Figure 16d, demonstrates why one expects a hot gap in the $(B - V, V)$ plane. However, the gap in Figure 16d refers only to ZAHB models. To understand where the gap would actually be observed in a CMD, we must include the HB evolution of the blue-hook and EHB models to brighter V magnitudes.

We show in Figure 17 the predicted location of the gap between the canonical EHB and blue-hook models, compared to the Bedin et al. (2000) luminosity function (shown as filled points with error bars). To derive the theoretical luminosity function in Figure 17b, we first assumed that the EHB and blue-hook models were distributed uniformly in V along the ZAHB (see Figure 17a). In addition, we adopted a bin size of

0.15 mag in V to be consistent with the Bedin et al. (2000) analysis. The total number of stars in the ZAHB distribution was normalized so that the theoretical HB distribution in Figure 17a had approximately the same number of stars as the Bedin et al. (2000) luminosity function from $19 \leq V \leq 21$ mag. The V magnitudes of the blue-hook models in Figure 17a were determined from the ZAHB luminosities of the He+C blue-hook models with $0.818 \leq \eta_R \leq 0.936$. The gap in the ZAHB distribution at $V \sim 20.5$ mag corresponds to the gap between the canonical ZAHB and He+C blue-hook models in Figure 16d.

The ZAHB models in Figure 17a will evolve towards higher luminosities until, by the end of the HB phase, they are ~ 0.5 mag brighter in V than at the ZAHB. In order to include this HB evolution, we distributed each of the ZAHB models in Figure 17a uniformly in time over its evolutionary track. These evolved HB models were then added to the appropriate luminosity bin to obtain the theoretical HB distribution shown in Figure 17b.

Our theoretical luminosity function agrees well with the Be-

din et al. (2000) data, given the unknown mass distribution on the HB and the uncertainties in translating the theoretical models to the observational plane. In particular, we note the good agreement between the predicted and observed location of the EHB gap. These results support the possibility that the gap within the EHB of NGC 2808 is due to the dichotomy between the blue-hook and canonical EHB models.

It is worth stressing that the gap within the EHB will only be apparent if the blue-hook stars have mixed envelopes. As shown in Figure 16*d*, if the blue-hook stars have envelopes with the normal cluster abundances, the blue-hook stars pile up near the end of the canonical ZAHB, with no gap between the canonical EHB and blue-hook stars. Whitney et al. (1998) argued that such an effect could explain the gap between the EHB and BHB in ω Cen. They only considered blue-hook stars with normal atmospheres, and showed that the range of η_R giving rise to the blue-hook stars was larger than the range of η_R populating the HB between the EHB and BHB; this effect would be exaggerated for the more metal-rich component of the ω Cen metallicity distribution (see D’Cruz et al. 1996). Thus, the region between the EHB and BHB would appear underpopulated, and then there would be a clump of stars at the hot end of the EHB (the blue-hook stars). However, the above analysis suggests that the dichotomy between the blue-hook and EHB stars causes the hottest gap within the EHB distribution, not the gap between the EHB and BHB, which therefore remains unexplained. From Figure 15 of Bedin et al. (2000), we see that there are more canonical EHB stars than blue-hook stars, even though the range in η_R that populates the canonical EHB is small. The gap between the EHB and BHB, at $V \approx 18.5$ mag, is too bright to be due to a build up of blue-hook stars near the hot end of the canonical ZAHB.

We have no plausible explanation for the EHB-BHB gap, which is very obvious in our STIS CMD, at $m_{FUV} - m_{NUV} \approx -1$ mag. However, an inspection of Figure 4 may offer a possible clue for the EHB-BHB gap. The HB stars that should fall in this gap are produced (in our models) by $\eta_R \approx 0.740$. This value of η_R falls in the transition between stars that flash at the RGB tip and those stars that flash as they are peeling away from the RGB (compare panels *b* and *c* in Figure 4).

8. IMPLICATIONS

8.1. *The Origin of Field He-sdB and He-sdO Stars*

The analysis presented herein offers a possible explanation for the subluminescent EHB stars seen in the globular clusters NGC 2808 and ω Cen. We have shown that stars evolving with high mass-loss on the RGB will undergo a late helium-core flash on the WD cooling curve that leads to convective flash mixing of the envelope. When these stars begin stable core He-burning, they will do so at temperatures significantly hotter than the hot end of the canonical EHB.

In the Galactic field, hot HB stars are observed spectroscopically as sdB and sdO stars (see Green, Schmidt, & Liebert 1986 for one version of the subdwarf classification scheme). Many sdO stars show enhanced helium, and those that do tend to show enhanced carbon as well (Lemke et al. 1997). Only a small fraction ($\sim 5\%$) of sdB stars show enhanced helium (Jeffery et al. 1996), but again, those that do also show strong carbon lines (e.g., Moehler et al. 1990). The sdO and sdB stars that do not have enhanced helium tend to be extremely deficient in their abundances of helium and most heavy metals. These deficiencies are attributed to gravitational settling.

Flash mixing would provide a possible explanation for why some sdB and sdO stars are helium- and carbon-enhanced, while others are depleted. Stars at $T_{\text{eff}} \lesssim 30,000$ K tend to be classified as sdB, and stars at $T_{\text{eff}} \gtrsim 40,000$ K tend to be classified as sdO, with the range $30,000 \lesssim T_{\text{eff}} \lesssim 40,000$ K variably classified as sdO, sdB, or sdOB. Because flash mixing on the WD cooling curve produces stars that are significantly hotter than the canonical EHB, one would expect more sdO stars to show helium and carbon enhancement than sdB stars, as observed. Note that we have no evidence for subluminous EHB stars or an EHB gap in the $\log T_{\text{eff}} / \log g$ plane in the Galactic field, nor do we have flash-mixed models for metal-rich stars; it is too early to say how much of a role these flash-mixed stars play in the Galactic field population, but these matters deserve further investigation.

The role of flash mixing in the field population might be partly obscured by several processes. If metallicity plays a role in RGB mass loss, the difference in metallicity between the field population and the globular cluster population may affect the properties of the flash-mixed HB models. For example, the more heterogeneous compositions of the field population might obscure an EHB gap that would otherwise be evident in a single metallicity stellar population. Also, the binary fraction in the field subdwarf population is unusually high (e.g., Maxted et al. 2001), which suggests that binarism might play a role in the formation of the field subdwarfs. In contrast, the fraction of EHB stars in NGC 2808 relative to the total HB population does not appear to vary radially (Walker 1999; Bedin et al. 2000), suggesting that these EHB stars are the products of single star evolution. The same is also true for ω Cen, which has the largest known population of EHB stars of any globular cluster (D’Cruz et al. 2000). Such possible differences in origin might also affect the evidence for flash mixing. Finally, gravitational settling of helium and carbon is very likely to obscure the evidence of flash mixing in some fraction of the hot HB stars, especially if the envelope should contain a small residual amount of hydrogen, and this settling might itself be affected by metallicity and binarism.

8.2. *Pulsating Subdwarfs*

The existence of pulsating sdB stars was predicted theoretically by Charpinet et al. (1996); subsequent observations by Kilkenny et al. (1997) of a binary sdB star, EC 14026-2647, proved their existence. More pulsating sdB stars were soon found (see O’Donoghue et al. 1999 and references therein), and the class is now referred to as EC 14026 stars or sdBV stars. Spectroscopy of these stars shows solar iron abundance even though other metals are greatly depleted (Heber et al. 2000). The enhancement of iron relative to other metals is of particular interest, because iron opacity is thought to be the pulsation driving mechanism (Charpinet et al. 1997).

Because the pulsating sdB stars tend to lie near $T_{\text{eff}} \sim 35,000$ K (O’Donoghue et al. 1999), some fraction may have been formed by a late helium-core flash on the WD cooling curve. Because flash mixing would greatly enhance the abundances of He and C in the envelope, this may affect the pulsations of such stars. The calculations of Charpinet et al. (1997) assume a hydrogen-rich envelope, but it would be interesting to see what is expected for a flash-mixed envelope.

8.3. *Observational Tests*

Although the optical and UV CMDs of NGC 2808 are consistent with a population of flash-mixed blue-hook stars near the

hot end of the canonical EHB, spectroscopic observations are required to fully explore the nature of the subluminal stars and validate the flash-mixing scenario we have described. Such observations are ideally suited to STIS, because one would want to observe stars that occupy various regions in the STIS UV CMD (stars along the BHB, EHB, and below the EHB). The center of NGC 2808 is too crowded to observe well from the ground, but is easily and efficiently available to STIS, because multiple stars can be placed in its long slits. Furthermore, many abundance diagnostics for both the light elements and heavier metals are available in the UV; thus UV spectroscopy can demonstrate if carbon and helium are enhanced relative to the other elements. We intend to investigate these stars further with STIS spectroscopy.

As explained in §4.3, our calculations cannot accurately determine if a small amount of residual hydrogen might be left in the stellar envelope when a star undergoes flash mixing. This issue can only be settled by detailed stellar structure calculations that include the energetics of the proton burning during the flash mixing phase. Because of the high gravity in the blue-hook stars, gravitational settling may bring any residual hydrogen to the surface. Our calculations show that a thin veneer of hydrogen ($\sim 10^{-6} M_{\odot}$) at the surface, as indicated by the diffusion calculations of Fontaine & Chayer (1997), would not greatly change the effective temperature of the blue-hook stars: they would still lie near $T_{\text{eff}} \approx 36,000$ K. However, the spectrum produced by a star with such a thin hydrogen veneer may not show the strong abundance enhancements predicted by the flash-mixing scenario, and instead may look much like a canonical EHB star with a very small envelope mass. These stars should still lie below the EHB in a UV CMD, due to the larger bolometric correction, but they will be considerably bluer than the flash-mixed blue-hook models shown in Figure 15.

Evidence for the flash-mixing scenario might also be provided by studying their post-HB progeny. As noted in §3.4, the STIS CMD shows a string of 9 stars that lie hotter and brighter than the hot end of the HB, in good agreement with theoretical lifetimes that predict ~ 9 post-HB stars corresponding to the 46 subluminal EHB stars. Figure 15 shows the post-HB evolution for a flash-mixed star; the predicted evolution does not reach as bright and hot as observed for the 9 candidate stars. However, given the uncertainty in the surface abundance of the flash-mixed stars (which may change due to diffusion as the stars evolve toward higher T_{eff} and lower gravity), we consider at least plausible the identification of the 9 candidate stars as the AGB-Manqué progeny of flash-mixed stars. A spectroscopic search for greatly enhanced carbon and helium abundances in these 9 hot stars could provide confirmation.

9. SUMMARY

Our UV CMD of NGC 2808 reveals a significant population of hot stars directly below the canonical ZAHB. Like those stars on the canonical HB, the subluminal stars may be in a core He-burning phase of evolution, but one that originates in

a late helium flash on the WD cooling curve. Our evolution models show that such a late flash will mix the hydrogen envelope with the helium core, which greatly enhances the envelope helium and carbon abundances. We have computed new model atmospheres and synthetic spectra for these flash-mixed stars, which show that these “blue-hook” stars should have lower luminosities and dramatically different envelope abundances than their counterparts on the canonical HB. These abundance enhancements would be detectable in far-UV spectroscopic observations with HST.

D’Cruz et al. (2000) invoked blue-hook stars to explain the subluminal HB stars in their ($F160BW - F555W$, $F555W$) CMD of ω Cen. However, it was difficult to explain the ~ 0.7 mag reduction in far-UV luminosity of these stars, because D’Cruz et al. (2000) assumed that there was no change in the mass or composition of the hydrogen-rich envelope in their models during the helium flash; their explanation, based on a small decrease in core mass, only reduces the bolometric luminosity by ~ 0.1 mag. However, their WFPC2/F160BW bandpass overlaps with our STIS/FUV bandpass, and is sensitive to the same opacity effects discussed here; if blue-hook stars have enhanced helium and carbon, this would explain why the subluminal HB stars in ω Cen extend to such faint far-UV luminosities below the canonical ZAHB.

Previous observations of NGC 2808 have also reported several gaps in the HB distribution (Sosin et al. 1997; Bedin et al. 2000). We have demonstrated that the hottest gap is likely due to the differences between the canonical EHB stars and the blue-hook population. The location of these blue-hook stars, relative to the canonical EHB, will vary with the bandpasses used for a CMD. In the STIS UV CMD, the blue-hook stars lie below the canonical EHB and are not separated by a gap; in optical CMDs, the blue-hook stars appear as a hot extension of the canonical EHB, separated by a prominent gap.

Besides ω Cen and NGC 2808, the only other globular cluster reported to have a significant EHB population fainter than $M_V = 4.5$ mag is NGC 6273 (Piotto et al. 1999). Thus flash-mixed stars probably do not comprise a significant fraction of the hot HB stars in classical EHB globular clusters such as NGC 6752 or M13, in which nearly all the EHB stars have $M_V < 4.5$ mag. However, even non-EHB clusters might have a small number of stars that experience a late helium-flash. As noted earlier, Moehler et al. (1997) report spectroscopy of an EHB star in M15 with $M_V = 4.7$ mag and a helium abundance of $N_{\text{He}}/(N_{\text{H}} + N_{\text{He}}) = 0.87$. This star is an excellent candidate for being a product of a late helium-core flash.

Support for this work was provided by NASA through the STIS GTO team funding. TMB gratefully acknowledges support at GSFC by NAS 5-6499D. AVS gratefully acknowledges support from NASA Astrophysics Theory Proposal NRA-99-01-ATP-039. We thank M.A. Wood for making his white dwarf cooling sequences publicly available.

REFERENCES

- Asplund, M., Lambert, D.L., Kipper, T., Pollacco, D., & Shetrone, M.D. 1999, *A&A*, 343, 507
 Baily, C. D. 1992, *ApJ*, 392, 519
 Bedin, L.R., Piotto, G., Zoccali, M., Stetson, P.B., Saviane, I., Cassisi, S., & Bono, G. 2000, *A&A*, 363, 159
 Behr, B.B., Cohen, J.G., & McCarthy, J.K. 2000, *ApJ*, 531, L37
 Behr, B.B., Cohen, J.G., McCarthy, J.K., & Djorgovski, S.G. 1999, *ApJ*, 517, L135
 Bertelli, G., Bressan, A., Chiosi, C., Fagotto, F., & Nasi, E. 1994, *A&AS*, 106, 275
 Blöcker, T. 2001, *Ap&SS*, 275, 1
 Bohlin, R. 1999, in STIS Instrument Science Report 1999-07: Changes in Sensitivity of the Low Dispersion Modes (Baltimore: STScI)
 Burstein, D., & McDonald, L.H. 1975, *AJ*, 80, 17
 Caloi, V. 1990, *A&A*, 232, 67
 Caloi, V. 1999, *A&A*, 343, 904

- Cardelli, J.A., Clayton, G.C., & Mathis, J.S. 1989, 345, 245
 Carney, B.W. 1996, PASP, 108, 900
 Castellani, M., & Castellani, V. 1993, ApJ, 407, 649
 Charpinet, S., Fontaine, G., Brassard, P., Chayer, P., Rogers, F.J., Iglesias, C.A., & Dorman, B. 1997, ApJ, 483, L123
 Charpinet, S., Fontaine, G., Brassard, P., & Dorman, B. 1996, ApJ, 471, L103
 Chieffi, A., Straniero, O., & Salaris, M. 1991, in ASP Conf. Ser. 13, The Formation and Evolution of Star Clusters, ed. K. Janes, (San Francisco: ASP), 219
 Clement, C., & Hazen, M. 1989, AJ, 97, 414
 Cunto, W., Mendoza, C., Ochsenbein, F., & Zeppen, C.J. 1993, A&A, 275, L5
 D’Cruz, N.L., Dorman, B., Rood, R.T., & O’Connell, R.W. 1996, ApJ, 466, 359
 D’Cruz, N.L., O’Connell, R.W., Rood, R.T., Whitney, J.H., Dorman, B., Landsman, W.B., Hill, R.S., Stecher, T.P., & Bohlin, R. 2000, ApJ, 530, 352
 Ferraro, F.R., Clementini, G., Fusi Pecci, F., Buonanno, R., & Alcaino, G. 1990, A&AS, 84, 59
 Ferraro, F.R., Messineo, M., Fusi Pecci, F., de Palo, M.A., Straniero, O., Chieffi, A., & Limongi, M. 1999, AJ, 118, 1738
 Ferraro, F.R., Paltrinieri, B., Fusi Pecci, F., Rood, R.T., & Dorman, B. 1998, ApJ, 500, 311
 Fontaine, G., & Chayer, P. 1997, in The Third Conference on Faint Blue Stars, ed. A.G.D. Phillip, J. Liebert, & R.A. Saffer (Schenectady: L. Davis Press), 169
 Fruchter, A.S., & Hook, R.N. 1998, PASP, submitted, astro-ph/9808087
 Fusi Pecci, F., & Bellazzini, M. 1997, in The Third Conference on Faint Blue Stars, ed. A.G.D. Phillip, J. Liebert, & R.A. Saffer (Schenectady: L. Davis Press), 255
 Gonzalez, G., Lambert, D.L., Wallerstein, G., Rao, N.K., Smith, V.V., & McCarthy, J.K. 1998, ApJS, 114, 133
 Green, R.F., Schmidt, M., & Liebert, J. 1986, ApJS, 61, 305
 Grundahl, F., Catelan, M., Landsman, W.B., Stetson, P.B., & Andersen, M.I. 1999, ApJ, 524, 242
 Harris, W.E. 1974, ApJ, 192, L161
 Heber, U., Reid, I.N., & Werner, K. 2000, A&A, 363, 198
 Herwig, F. 2001a, Ap&SS, 275, 15
 Herwig, F. 2001b, Ap&SS, in press, astro-ph/0103003
 Herwig, F. 2001c, Ap&SS, in press, astro-ph/0103004
 Herwig, F., Blöcker, T., Langer, N., & Driebe, T. 1999, A&A, 349, L5
 Herwig, F., & Langer, N. 2001, Nucl. Phys. A, in press, astro-ph/0010120
 Hubeny, I., & Lanz, T. 1995, ApJ, 439, 875
 Hubeny, I., Lanz, T., & Jeffery, C.S. 1994, Newsl. Anal. Astron. Spectra, 20, 30
 Iben, I., Jr. 1976, ApJ, 208, 165
 Iben, I., Jr. 1984, ApJ, 277, 333
 Iben, I., Jr. 1995, Physics Reports, 250, 1
 Iben, I., Jr., Kaler, J.B., Truran, J.W., & Renzini, A. 1983, ApJ, 264, 605
 Iben, I., Jr., & MacDonald, J. 1995, in White Dwarfs, ed. D. Koester & K. Werner (Heidelberg: Springer), 48
 Jeffery, C.S., Heber, U., Hill, P.W., Driezler, S., Drilling, J.S., Lawson, W.A., Leuenhagen, U., & Werner, K. 1996, in Hydrogen-Deficient Stars, ed. C.S. Jeffery & U. Heber (San Francisco: ASP), 471
 Kaluzny, J., Kubiak, M., Szymanski, M., Udalski, A., Krzeminski, W., Mateo, M., & Stanek, K. 1997, A&AS, 122, 471
 Kilkenny, D., Koen, C., O’Donoghue, D., & Stobie, R.S. 1997, MNRAS, 285, 640
 Kimble, R. A., et al. 1998, ApJ, 492, 83
 Knigge, C., Shara, M.M., Zurek, D.R., Long, K.S., & Gilliland R.L., in Stellar Collisions, Mergers, and their Consequences, ASP Conference Series, in press, astro-ph/0012187
 Kurucz, R. L. 1993, CD-ROM 13, ATLAS9 Stellar Atmosphere Programs and 2 km/s Grid (Cambridge: Smithsonian Astrophys. Obs.)
 Landsman, W.B., Sweigart, A.V., Bohlin, R.C., Neff, S.G., O’Connell, R.W., Roberts, M.S., Smith, A.M., & Stecher, T.P. 1996, ApJ, 472, L93
 Landsman, W.B., et al. 2001, in preparation.
 Lee, Y.-W., Joo, J.-M., Sohn, Y.-J., Rey, S.-C., Lee, H.-C., & Walker, A.R. 1999, Nature, 402, 55
 Lemke, M., Heber, U., Napiwotzki, R., Drizler, S., & Engels, D. 1997, in The Third Conference on Faint Blue Stars, ed. A.G.D. Phillip, J. Liebert, & R.A. Saffer (Cambridge: Cambridge University Press), 375
 Lindler, D. 1999, CALSTIS Reference Guide, <http://hires.gsfc.nasa.gov/stis/docs/calstis/>
 Maxted, P.F.L., Heber, U., Marsh, T.R., & North, R.C. 2001, MNRAS, in press, astro-ph/0103342
 Moehler, S., Heber, U., & Durrell, P.R. 1997, A&A, 317, L83
 Moehler, S., Richtler, T., de Boer, K.S., Dettmar, R.J., & Heber, U. 1990, A&AS, 86, 53.
 Moehler, S., Sweigart, A.V., Landsman, W.B., & Heber, U. 2000, A&A, 360, 120
 O’Donoghue, D., Koen, C., Kilkenny, D., Stobie, R.S., & Lynas-Gray, A.E. 1999, in The 11th European Workshop on White Dwarfs, ed. J.-E. Solheim & E.G. Meißas (San Francisco: ASP), 149
 Panei, J.A., Althaus, L.G., & Benvenuto, O.G. 2000, A&A, 353, 970
 Piotto, G., Zoccali, M., King, I.R., Djorgovski, S.G., Sosin, C., Rich, R.M., & Meylan, G. 1999, AJ, 118, 1727
 Reimers, D. 1975, Mém. Roy. Soc. Liège, 8, 369
 Reimers, D. 1977, A&A, 57, 395
 Renzini, A. 1990, in Confrontation Between Stellar Pulsation and Evolution, ed. C. Cacciari & G. Clementini (San Francisco: ASP), 549
 Rich, R. M., et al. 1997, ApJ, 484, L25
 Robinson, R. 1997, in “Examining the STIS Point Spread Function,” http://hires.gsfc.nasa.gov/stis/postcal/quick_reports/
 Rood, R.T., Crocker, D.A., Fusi Pecci, F., Ferraro, F.R., Clementini, G., & Buonanno, R. 1993, in The Globular Clusters-Galaxy Connection., ed. G.H. Smith & J.P. Brodie (San Francisco: ASP), 218
 Rutledge, G.A., Hesser, J.E., & Stetson, P.B. 1997, PASP, 109, 907
 Saffer, R.A., Bergeron, P., Koester, D., & Liebert, J. 1994, ApJ, 432, 351
 Salaris, M., Chieffi, A., & Straniero, O. 1993, ApJ, 414, 580
 Sanders, R.H. 1967, ApJ, 150, 971
 Sosin, C., Dorman, B., Djorgovski, S.G., Piotto, G., Rich, R.M., King, I.R., Liebert, J., Phinney, E.S., & Renzini, A. 1997, ApJ, 480, L35
 Sweigart, A.V. 1974, ApJ, 189, 289
 Sweigart, A.V. 1994a, ApJ, 426, 612
 Sweigart, A.V. 1994b, in Hot Stars in the Galactic Halo, ed. S.J. Adelman, A.R. Ugren, & C.J. Adelman (Cambridge: Cambridge University Press), 17
 Sweigart, A.V. 1997, in The Third Conference on Faint Blue Stars, ed. A.G.D. Phillip, J. Liebert, & R.A. Saffer (Schenectady: L. Davis Press), 3
 Sweigart, A.V., & Gross, P.G. 1976, 32, 367
 VandenBerg, D.A. 2000, ApJS, 129, 315
 VandenBerg, D.A., Swenson, F.J., Rogers, F.J., Iglesias, C.A., & Alexander, D.R. 2000, ApJ, 532, 430
 Walker, A.R. 1999, AJ, 118, 432
 Whitney, J.H., et al. 1994, AJ, 108, 1350
 Whitney, J.H., Rood, R.T., O’Connell, R.W., D’Cruz, N.L., Dorman, B., Landsman, W.B., Bohlin, R.C., Roberts, M.S., Smith, A.M., & Stecher, T.P. 1998, ApJ, 495, 284
 Wood, M.A. 1995, in Proceedings of the 9th European Workshop on White Dwarfs, eds. D. Koester and K. Werner (Berlin: Springer-Verlag), 41
 Woodgate, B. E., et al. 1998, PASP, 110, 1183
 Zinn, R., & West, M.J. 1984, ApJS, 55, 45

TABLE 2: Photometric Catalog

RA ^a (J2000)	Decl. ^a (J2000)	m_{FUV} (mag)	Error (mag)	m_{NUV} (mag)	Error (mag)
9 12 00.0113	-64 51 47.334	16.43	0.02	16.92	0.01
9 12 00.1639	-64 51 50.573	16.29	0.02	16.97	0.01
9 12 00.1668	-64 51 53.261	16.73	0.03	17.13	0.02
9 12 00.2360	-64 51 49.498	16.41	0.01	16.94	0.01
9 12 00.2451	-64 51 50.912	17.34	0.03	18.85	0.04

NOTE— Table 2 is available only on-line as a machine-readable table. A portion is shown here for guidance regarding its form and content. Units of right ascension are hours, minutes, and seconds, and units of declination are degrees, arcminutes, and arcseconds.

^aThe relative astrometry is very accurate (tenths of a 0.025'' STIS pixel), but the absolute astrometry is subject to a 1–2'' uncertainty (associated with the position of the guide stars).